

To appear in the *Astrophysical Journal*

Theory and astrophysical consequences of a magnetized torus around a rapidly rotating black hole

Maurice H.P.M. van Putten

*LIGO Project, Massachusetts Institute of Technology, NW17-161, 175 Albany St.,
Cambridge, MA 02139-4307*

Amir Levinson

School of Physics and Astronomy, Tel Aviv University, Tel Aviv, Israel

ABSTRACT

We analyze the topology, lifetime, and emissions of a torus around a black hole formed in hypernovae and black hole-neutron star coalescence. The torus is ab initio uniformly magnetized, represented by two counter oriented current-rings, and develops a state of suspended accretion against a “magnetic wall” around the black hole. Magnetic stability of the torus gives rise to a new fundamental limit $\mathcal{E}_B/\mathcal{E}_k < 0.1$ for the ratio of poloidal magnetic field energy-to-kinetic energy, corresponding to a maximum magnetic field strength $B_c \simeq 10^{16} \text{G} (7M_\odot/M_H) (6M_H/R)^2 (M_T/0.03M_H)^{1/2}$. The lifetime of rapid spin of the black hole is effectively defined by the timescale of dissipation of black hole-spin energy E_{rot} in the horizon, and satisfies $T \simeq 40\text{s} (M_H/7M_\odot) (R/6M_H)^4 (0.03M_H/M_T)$ for a black hole of mass M_H surrounded by a torus of mass M_T and radius R . E_{rot} of the black hole. The torus converts a major fraction $E_{gw}/E_{rot} \sim 10\%$ into gravitational radiation through a finite number of multipole mass-moments, and a smaller fraction into MeV neutrinos and baryon-rich winds. At a source distance of 100Mpc, these emissions over $N = 2 \times 10^4$ periods give rise to a characteristic strain amplitude $\sqrt{N}h_{char} \simeq 6 \times 10^{-21}$. We argue that torus winds create an open magnetic flux-tube on the black hole, which carries a minor fraction $E_j/E_{rot} \simeq 10^{-3}$ in baryon-poor outflows to infinity. We conjecture that these are not high-sigma outflows owing, in part, to magnetic reconnection in surrounding current sheets. The fraction $E_j/E_{rot} \sim (1/4)(M_H/R)^4$ is standard for a universal horizon half-opening angle $\theta_H \simeq M_H/R$ of the open flux-tube. We identify this baryon poor

output of tens of seconds with GRBs with contemporaneous and strongly correlated emissions in gravitational radiation, conceivably at multiple frequencies. Ultimately, this leaves a black hole binary surrounded by a supernova remnant.

1. Introduction

Black holes surrounded by a magnetized torus or disk are believed to constitute the central engines that power various high-energy sources, notably active galactic nuclei, galactic microquasars, and gamma-ray bursts. The latter systems are thought to be the outcome of catastrophic events such as core-collapse in massive stars and black hole-neutron star coalescence (Eichler, et al. 1989; Woosley 1993; Paczynski 1991; Paczyński 1998), and are of interest as potentially the most extreme and short-lived black hole-torus systems.

We describe a theory for the topology, lifetime and emissions of a black hole-torus systems as a function of three parameters: the mass M_H of an extreme Kerr black hole, the radius R and the mass M_T of the torus. We shall do so largely by studying the torus by equivalence to pulsars, in both topology and ms rotation periods. The energy emissions are powered by the spin-energy of a Kerr black hole (Kerr 1963). Most of the black hole-luminosity – the rate at which the black hole deposits energy into its surroundings in all channels – is incident on the torus, which hereby creates a *major* energy output of the system. A *minor* energy output is released in baryon-poor outflows through an open magnetic flux-tube along the spin-axis of the black hole. The life-time of these black hole-torus systems is identified with the lifetime of rapid spin of the black hole in a state of suspended accretion (van Putten & Ostriker 2001) against a “magnetic wall” around the black hole (van Putten 1999). The suspended accretion state results from a strong coupling of the torus to the spin-energy of the black hole. We point out that this mechanism is based on a uniform magnetization of the torus, represented by two oppositely oriented current rings (van Putten 1999). This magnetization is a natural outcome of both black hole-neutron star coalescence and core-collapse in hypernovae.

In this paper, we quantify (1) the lifetime of rapid spin of the black hole in terms of a new magnetic stability criterion for the torus; (2) baryon-rich outflows from the torus at MeV temperatures; and (3) the fraction of black hole spin-energy in baryon-poor outflows through an open magnetic flux-tube on the black hole, created from outer layers of the inner torus magnetosphere by these torus winds.

The torus is luminous in various channels, which are strongly correlated by the properties of the torus: in gravitational radiation, winds, thermal and MeV neutrino emissions (van Putten 2001b; van Putten & Levinson 2002). Calorimetric constraints on the torus

winds hereby obtains predictions for the proposed emissions in gravitational radiation, while calorimetry on the gravitational wave emissions by upcoming gravitational wave-experiments obtains a method for identifying Kerr black holes as objects in nature (van Putten & Levinson 2002).

Gravitational radiation forms a major output of the system and the dominant output of the torus (van Putten 2001b; van Putten & Levinson 2002). This is emitted by a finite number of multipole mass moments in a torus of finite slenderness, due to the Papaloizou-Pringle instability (Papaloizou & Pringle 1984; van Putten 2002a) and, conceivably, other wave-modes in the torus. These emissions are candidate sources for the upcoming gravitational wave-experiments by laser interferometric instruments LIGO (Abramovici et al. 1992), VIRGO (Bradaschia et al. 1992), TAMA (Masaki et al. 2001) and GEO (e.g., Schutz & Papa (1999)), or by any of the bar or sphere detectors presently under construction. The frequency in gravitational radiation is determined by the keplerian frequency of the torus. The latter is strongly correlated to the output energy in torus winds. This suggests the possibility of performing calorimetry on the impact of these torus winds on the remnant stellar envelope (van Putten 2002b) and on supernova remnants, in order to constrain the expected frequency in gravitational radiation.

Baryon-poor outflows form a small fraction of the total output from the black hole through an open magnetic flux-tube (van Putten & Levinson 2002). We here attribute the formation of this open flux-tube to powerful baryon-rich torus winds, driven from the surface by escaping MeV neutrinos. This neutrino output provides the dominant cooling mechanism of the torus during the suspended accretion state, in addition to the energy release in gravitational waves. The fraction of rotational energy thus released is proportional to θ_H^4 , which is standard for a universal horizon half-opening angle θ_H of the inner tube. These outflows are probably not high-sigma, owing to magnetic reconnection in the interface between the baryon poor and baryon-rich winds in a surrounding outer flux-tube. The half-opening angle is possibly related to curvature in poloidal topology (van Putten 2002b).

Tentative observational evidence for a black hole-luminosity incident into surrounding matter in case of supermassive black holes is found in MCG-6-30-15 (Wilms et al. 2001), and in case of stellar mass black hole-candidates in the galactic source XTE J1650-500 (Miller et al. 2002). Independent observational evidence of the presence of magnetic fields remains elusive. We point out, however, that in our model heating of the torus is due to viscous shear between its inner and outer faces, possibly in the form of magnetohydrodynamical turbulence, which is different from electric dissipation as envisioned in Wilms et al. (2001).

In §2 and §3 we describe the topology and stability of the magnetosphere of a torus formed in black hole-neutron star coalescence and supernova, the suspended accretion state

around rapidly rotating black holes and the secular time-scale of its rapid spin. The formation of a finite number of multipole mass moments by the Papaloizou-Pringle instability in tori of finite slenderness is summarized in §4. Energy emissions in various channels by the torus are described in §5. We calculate the neutrino driven mass loss rate from the torus’ surface in §6. These baryon-rich torus winds have some implications for energy extraction from the black hole and the creation of open magnetic flux-tubes from outer layers in the inner torus magnetosphere. §7- §9 describe the structure of the inner flux-tube supported by the black hole, and dissipation by magnetic reconnection in its interface with the surrounding outer flux-tube. We conclude with observational consequences in §10.

2. Formation and structure of the torus magnetosphere

A torus formed in core-collapse of a massive star or black hole-neutron star coalescence will be magnetized with a remnant of the progenitor magnetic field. An aligned poloidal magnetic field in the progenitor star provides a magnetic moment density in the torus, aligned with its axis of rotation. Equivalently, the magnetic field in the torus is produced by two concentric current loops with opposite orientation. In the case of a torus formed from the break-up of a neutron star around a black hole, these two current loops form out of a single current loop representing the magnetization of the neutron star, upon stretching the latter around the black hole followed by a reconnection (see Fig. 1). Conceivably, the magnetic field in the torus is amplified by winding or a dynamo process. The stability of this magnetic field configuration is discussed in §3, and sets an upper limit of $B \simeq 10^{16}\text{G}$ on the field-strength.

Below, we outline the resulting magnetosphere of the black hole torus system in the force-free limit. For illustrative purposes we consider first the poloidal topology of the vacuum magnetic field configuration. We proceed by discussing the more realistic situation of a force-free magnetosphere, and show that the inner and outer face of the torus are each equivalent to a pulsar with, however, generally different angular velocities.

In the subsequent sections we shall consider some essential energetic aspects in greater detail. In particular, it will be shown that appreciable matter outflows are expected along open field lines to infinity, and a reconnection boundary is expected to form near the rotation axis. This may give rise to a non-force-free magnetic field in those regions.

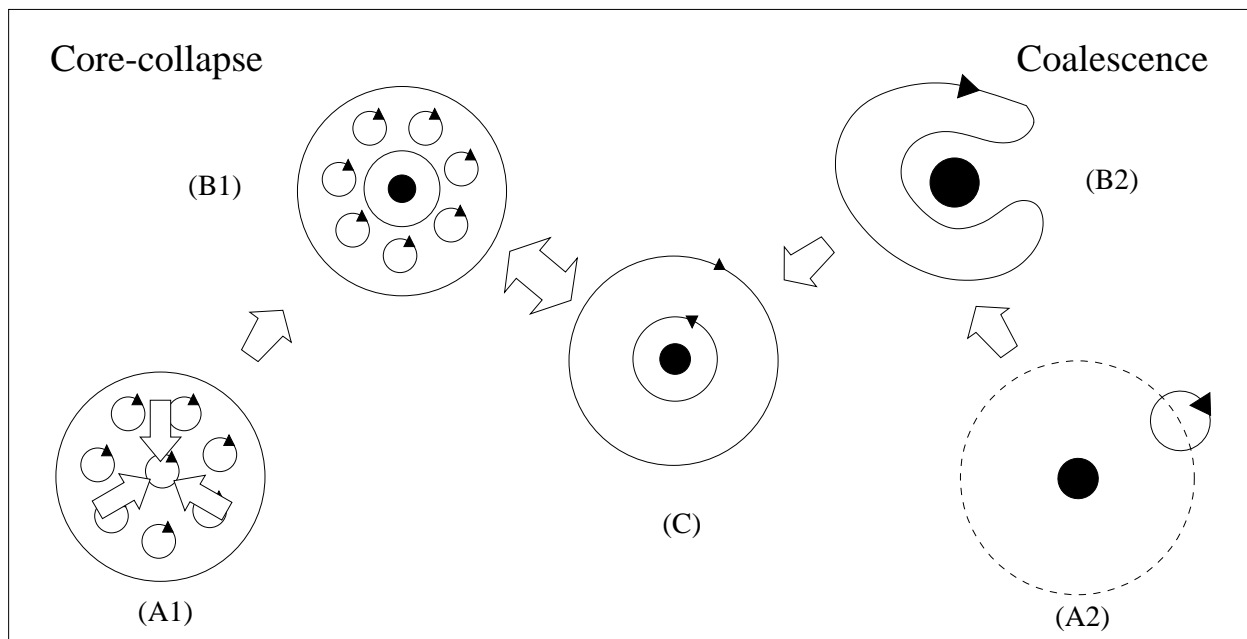


Fig. 1.— A uniformly magnetized torus around a black hole (C) is represented by two counter-oriented current rings in the equatorial plane. It forms a common end point of both core-collapse (A1,B1,C) and black hole-neutron star coalescence (A2,B2,C). Core-collapse (A1-B1) in a magnetized star results in a uniformly magnetized, equatorial annulus (C); tidal break-up (A2-B2) wraps the current ring representing the magnetic moment of a neutron star around the black hole which, following a reconnection, leaves the same (C).

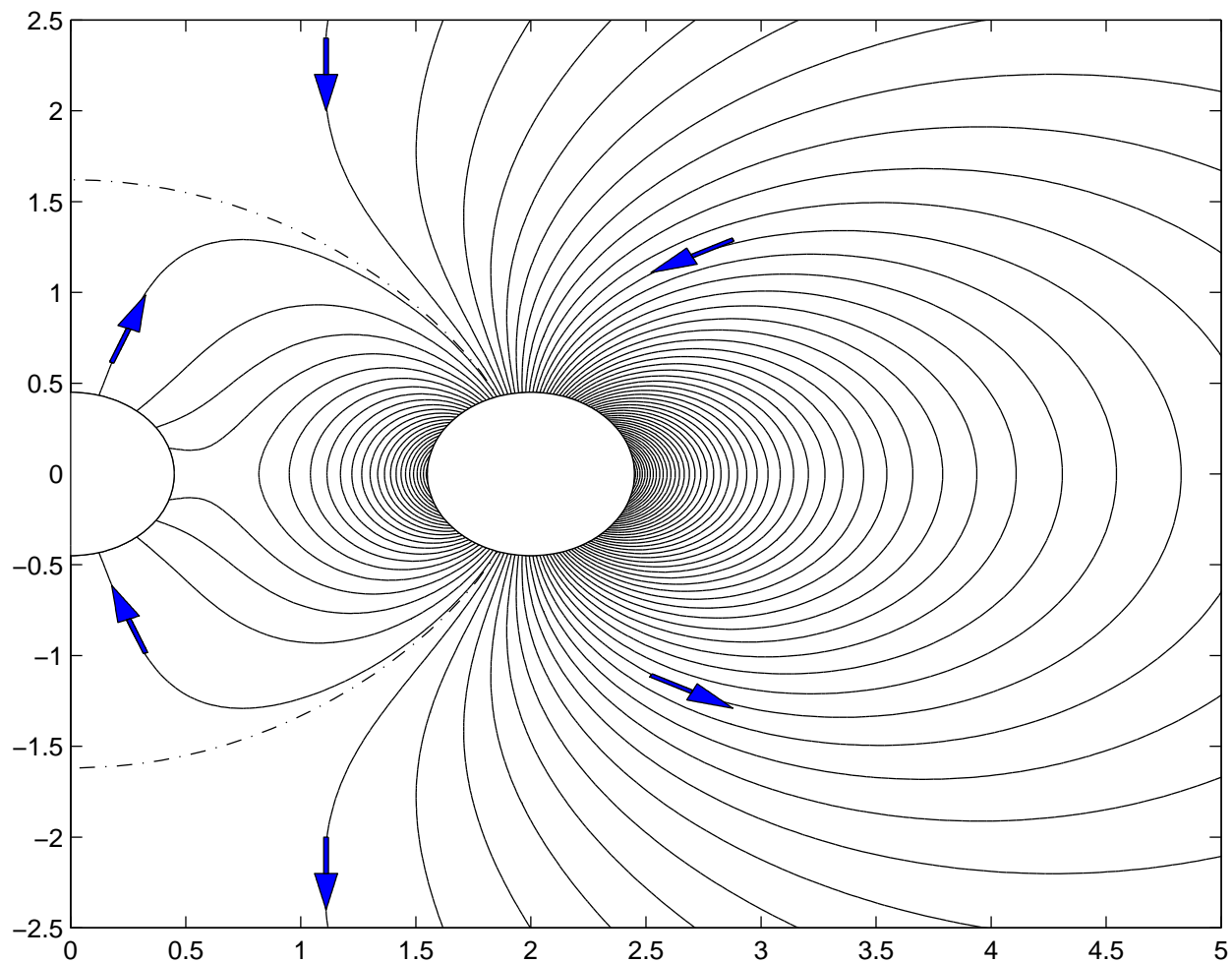


Fig. 2.— The poloidal topology of magnetic flux-surfaces in vacuum is illustrated in flat space-time, produced by two counter-oriented current rings representing a uniformly magnetized torus (*center*). The dashed line is the separatrix between the flux-surfaces supported by the inner and the outer faces of the torus. A Kerr black hole develops an equilibrium magnetic moment which preserves essentially uniform and maximal magnetic flux through its horizon.

2.1. Topology of the vacuum magnetic field

A uniform magnetization of the torus is approximately described by two counter-oriented current rings in the equatorial plane. A third current loop is associated with the black hole, representing its equilibrium magnetic moment in its lowest energy state (van Putten 2001b). This induced magnetic moment is oriented antiparallel to the magnetic moment of the torus, facilitating an essentially uniform and maximal horizon flux at arbitrary spin-rates. In flat space-time, the magnetic field produced by a superposition of current rings can be calculated analytically (Jackson 1975). The topology of this ab initio flat-spacetime vacuum magnetic field is shown in Fig. 2. As seen, at large radii (compared with the radius of the outer current ring) it quickly approaches a dipole solution. In the inner region the field lines intersect the horizon, giving rise to a strong coupling between the black hole and the inner face of the torus. This topology and flux-distribution is preserved in the face of general relativistic effects, as a result of the equilibrium magnetic moment of the black hole.

2.2. Equivalence to pulsars

By vacuum break-down, the flux-surfaces will evolve with electric charges to a largely force-free state similar to pulsars (Goldreich & Julian 1969). As a result, a magnetosphere develops which consists of conductive flux-surfaces and magnetic winds. The torus hereby supports an inner and an outer torus magnetosphere. These are equivalent in poloidal topology to pulsar magnetospheres, wherein the horizon of the black hole is equivalent to a compactified infinity with non-zero angular velocity (Fig. 3). This equivalence implies similar, causal interactions by magnetic winds acting on the inner and outer face of the torus.

In the force-free limit, the flux-surfaces in the outer/inner torus magnetosphere assume rigid corotation with the outer/inner face of the torus, by no-slip boundary conditions on the surface. Field-lines in the vicinity of the torus and the equatorial plane form a ‘bag’ of closed field-lines (both on the inner and the outer face) with no-slip/no-slip boundary conditions. The last closed field-line of the outer torus magnetosphere reaches the light-cylinder associated with the angular velocity of the outer face of the torus, similar to the last closed field-lines in pulsar magnetospheres. The last closed field-line of the inner torus magnetosphere reaches the inner light-surface (Znajek 1977) associated with the angular velocity of the inner face of the torus (Fig. 2 of van Putten (1999)). Beyond, field-lines are open, and extend to infinity or to the horizon of the black hole with no-slip/slip boundary conditions. The former are created by torus winds which cross the outer light cylinder.

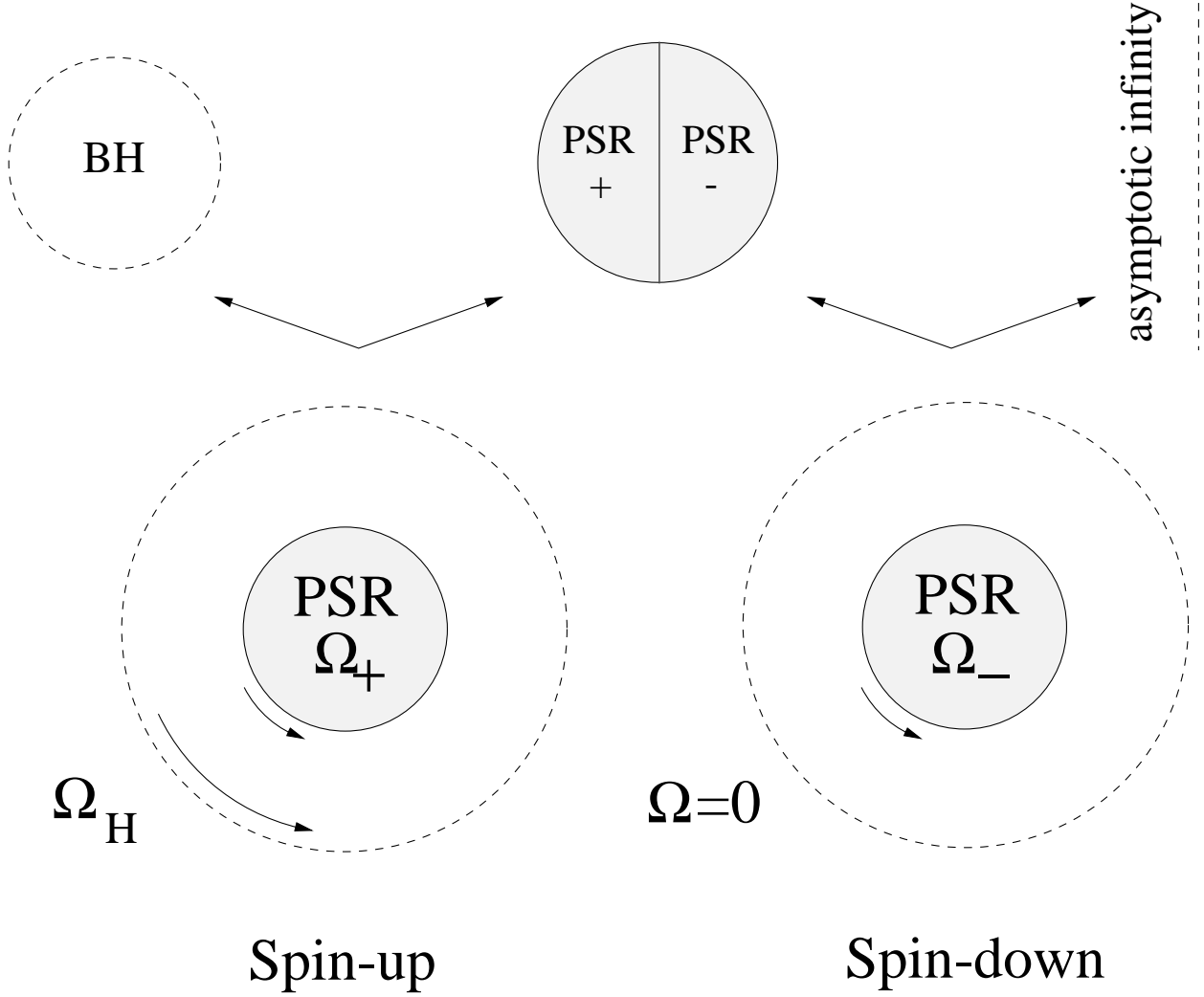


Fig. 3.— *Lower left.* The inner face of the torus (angular velocity Ω_+) and the black hole (angular velocity Ω_H) is equivalent to a pulsar surrounded by infinity with relative angular velocity $\Omega_H - \Omega_+$. By equivalence in poloidal topology to pulsar magnetospheres, the inner face receives energy and angular momentum from the black hole as a causal process, whenever $\Omega_H - \Omega_+ > 0$. *Lower right.* The outer face of the torus (angular velocity Ω_-) is equivalent to a pulsar with angular velocity Ω_- , and always loses energy and angular momentum, by the same equivalence.

2.3. Suspended accretion against a magnetic wall

Most of the black hole-luminosity is incident on the torus (van Putten 1999). The torque exerted on the inner face of the torus by the black hole is obtained by integrating the angular momentum flux $\mathcal{L}^r = F^{r\theta}F_{\phi\theta}/4\pi$ over the section of the horizon which is threaded by magnetic field lines that are anchored to the torus:

$$T_+ = 4\pi \int_{\theta_H}^{\pi/2} \sqrt{-g} \mathcal{L}^r d\theta = (\Omega_H - \Omega_+) \int_{\theta_H}^{\pi/2} \frac{\Sigma}{\rho^2} \sin \theta (F_{\phi\theta})^2 d\theta, \quad (1)$$

where eq. (A18) has been used. Here θ_H is the angle of the last field line that connects the torus and the horizon (see Fig. 3), Ω_+ and Ω_H are the angular velocities of the inner face of the torus and the black hole, respectively, and the metric components, ρ , Σ are defined in the appendix. In terms of the net poloidal magnetic flux associated with the open field lines in the torus, $2\pi A$, we may write $T_+ = (\Omega_H - \Omega_+) f_H^2 A^2$. Formally f_H is defined through eq. (1). Likewise, the torque exerted on the outer face by field lines that extend to infinity can be expressed as: $T_- = \Omega_- f_w^2 A^2$, where Ω_- is the angular velocity of the outer face of the torus, and f_w is the fraction of open field lines that extend to infinity. It is seen that when $\Omega_H > \Omega_+$ angular momentum is transferred from the black hole to the torus, tending to spin up the inner face, whereas in the slowly rotating case ($\Omega_H < \Omega_+$) the black hole receives angular momentum from the torus (Fig. 4). The outer face always loses angular momentum via a wind to infinity. By mechanical work, the magnetic torus winds to infinity and into the horizon carrying outgoing luminosities

$$L_{\pm} = \Omega_{\pm} T_{\pm}. \quad (2)$$

The inner face thus receives a fraction Ω_+/Ω_H of the maximum extractable power $\Omega_H T_+$ (Thorne et al. 1986); the rest dissipates on the horizon.

The positive and negative torques exerted on the inner and outer faces of the torus in the rapidly rotating case, give rise to a differential rotation of the torus. In steady state, a flow of angular momentum from the inner to the outer face is accomplished through shear forces. The nature of the latter is presumably electromagnetic (Balbus & Hawley 1992), stimulated by magneto-hydrodynamic instabilities (see §4). As a consequence, a fraction of the black hole spin down energy that is intercepted by the inner face is dissipated in the torus, heating it to MeV temperatures.

2.4. Frame-dragging and electric charge distribution

The electric charge distribution can be obtained from Maxwell's equation: $F^{t\mu}_{;\mu} = 4\pi j^t$. Assuming the radial magnetic field, $B_r = -F_{\phi\theta}/(\Sigma \sin \theta)$, to be independent of θ , we obtain

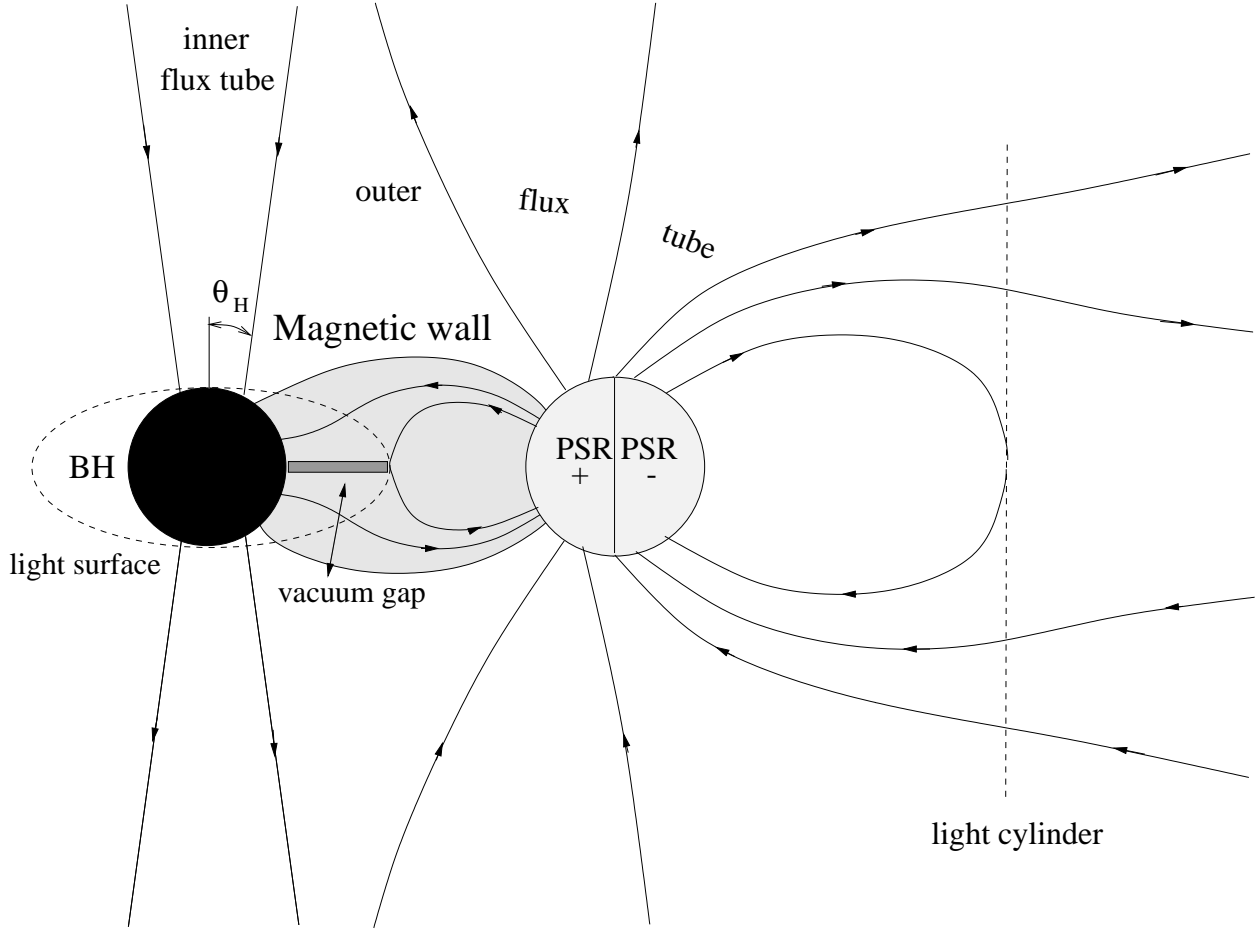


Fig. 4.— Schematic illustration of the poloidal topology of the magnetosphere of a torus surrounding a rapidly rotating black hole. Balance of the input on the inner face and the output through the outer face and other losses results in a suspended accretion state. The inner torus magnetosphere hereby represents a magnetic wall around the black hole, whereby the torus receives energy and angular momentum from the black hole by equivalence to pulsars. The associated horizon Maxwell stresses (Blandford & Znajek 1977) and Maxwell stresses on the inner face of the torus (van Putten 1999) are mediated by poloidal currents, which close over a vacuum gap in an annulus of vanishing magnetic field. The torus hereby receives a *major* fraction of the black hole-spin energy, catalyzing this into gravitational radiation, winds, thermal and MeV neutrino emissions. A baryon-poor inner flux-tube serves as an artery for a *minor* fraction of black hole-spin energy. The dashed line indicates the light cylinder of the outer face of the torus. The lifetime of the system is set by the lifetime of rapid spin of the black hole.

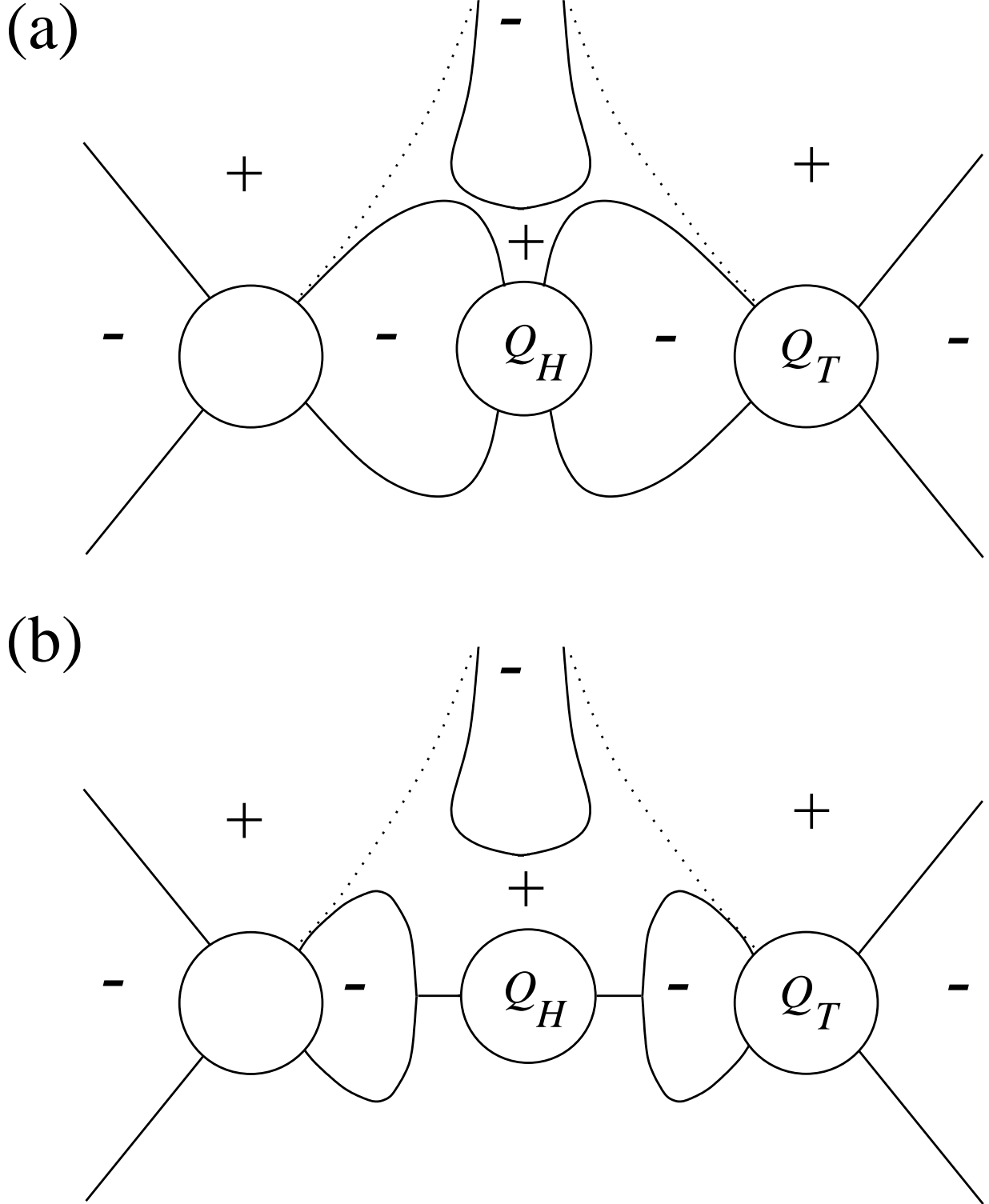


Fig. 5.— Schematic of the charge-distribution in a torus magnetosphere around Kerr black holes, showing two bifurcations from non-rotation (dotted line). Frame-dragging introduces a sign-change in flux-tubes which rotate slower than the black hole (a). Black holes rotating faster than the torus produce an inner light surface, and hence an annulus of $B = 0$ (b). Equilibrium magnetic moments of the black hole and the torus correspond to charges Q_H and Q_T with opposite sign (Q_T is analogous to pulsar charges Cohen et al. (1975))

from eq. (A19) the Goldreich-Julian charge density near the horizon, on field lines that emanate from the inner face:

$$\rho_e = \alpha^2 j^t = -\frac{(\Omega_+ + \beta)B_r \cos \theta}{2\pi}, \quad (3)$$

where β is defined below eq. (A1), and equals $-\Omega_H$ on the horizon. We find that for $\Omega_H > \Omega_+$, the charge density changes sign on field lines threading the horizon. The same holds true also for the inner flux tube that extend to infinity (see discussion following eq. [44]).

The charge-distribution (3) represents a bifurcation from the magnetosphere around a Schwarzschild black hole. Ingoing horizon boundary conditions and outgoing boundary conditions at infinity may hereby carry a continuous electric current. If the black hole rotates slower than the inner face of the torus, the inner light-surface is absent and the sign of the charge-distribution near the torus carries through to the horizon (Fig. 5a). If the black hole rotates faster than the inner face of the torus, the inner light-surface becomes apparent (a bifurcation from slow rotation) and, by forgoing arguments, introduces a sign change in the charge-distribution (Fig. 5b).

3. The lifetime of rapid spin of the black hole

A magnetized torus of a few tenths of solar masses around a stellar mass black hole of about $7M_\odot$ is subject to magnetic self-interaction and a stabilizing tidal interaction in the central potential well. We here derive limits on the average strength of a poloidal magnetic field which can be supported by the torus. We do not consider the problem of stability of a poloidal magnetic field itself, such as the magnetorotational (MRI) instability. A limit on the energy in poloidal magnetic field defines a lower bound on the lifetime of rapid spin of the black hole.

In regards to wave-motion within the equatorial plane, the contribution of poloidal magnetic fields is that of magnetic pressure, which is generally stabilizing on the motion of the fluid. In regards to poloidal wave-motion, a poloidal magnetic field generally conspires towards instabilities. This can be calculated by partitioning the torus in a finite number of fluid elements with current loops, representing local magnetic moments. The two leading-order partitions are shown in configurations C and B1 of Fig. 1, for which we derive critical magnetic field-strengths. The first is subject to magnetic tilt instability between the inner and the outer face, and the second is subject to a magnetic buckling instability.

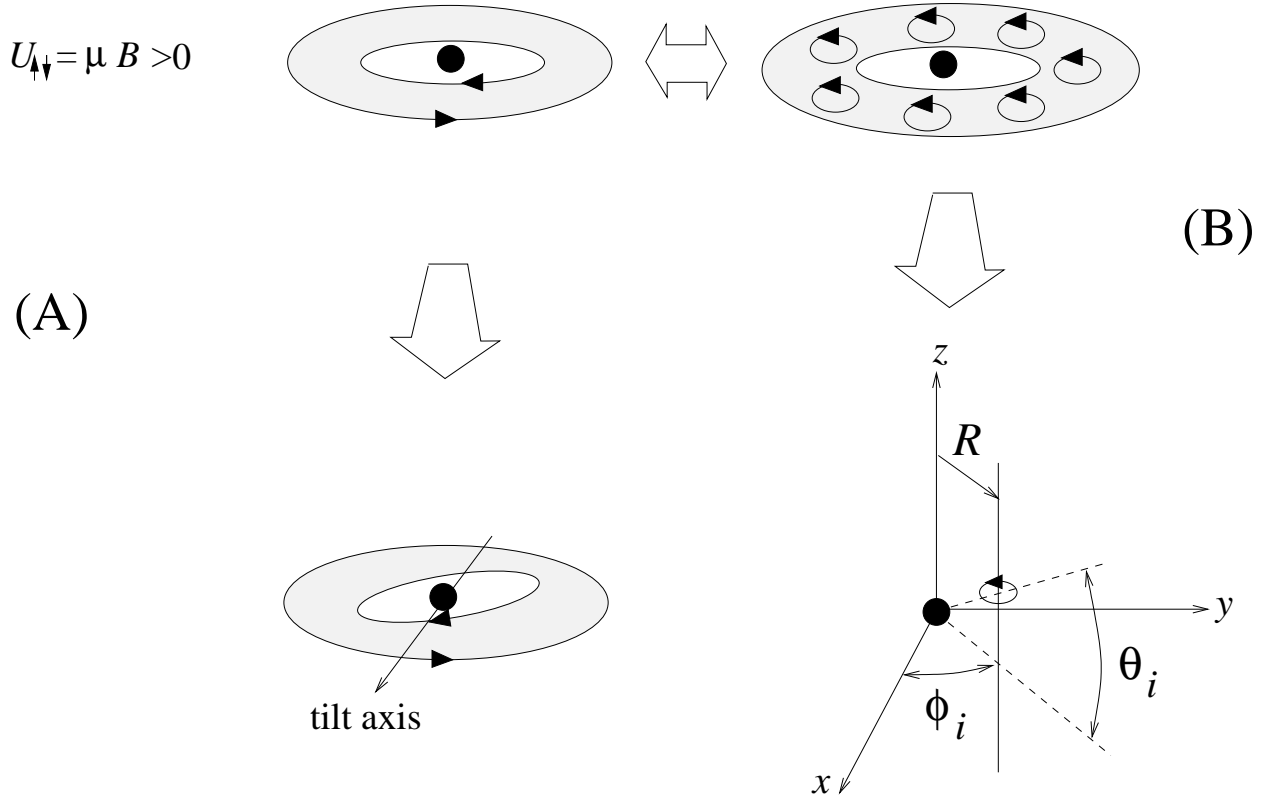


Fig. 6.— A uniformly magnetized torus is in its highest magnetic energy state. The two alternative leading-order partitions of the current distribution (*top*) have unstable poloidal modes, described by a relative tilt between the two current rings towards alignment (A) or towards buckling (B), characterized by perturbations out of the equatorial plane with poloidal angles $\theta_i \neq \theta_j$. We consider vertical displacements of fluid elements along a cylinder of radius R . Their wave-modes are stabilized by the tidal gravitational field of the central black hole, provided the magnetic field-strength remains below a critical value on the order of 10^{16}G . This gives rise to a minimum lifetime of rapid spin of the black hole on the order of tens of seconds, consistent with the redshift-corrected durations of long GRBs.

3.1. A magnetic tilt instability

Following C in Fig. 1, consider the magnetic interaction energy of a pair of concentric current rings, given by

$$U_\mu(\theta) = -\mu B \cos \theta. \quad (4)$$

Here, μ is the magnetic moment of the inner ring, B is the magnetic field produced by the outer ring, and θ denotes the angle between μ and B . Note that $U_\mu(\theta)$ has a period 2π , is maximal (minimal) when μ and B are antiparallel (parallel; see Fig. 6). Consider tilting a fluid element of a ring out of the equatorial plane to a height z approximately along a cylinder of radius R . (This is different from tilting a rigid ring, whose elements move on a sphere). A tilt hereby changes the distance to central black hole to $\rho = \sqrt{R^2 + z^2} \simeq R(1 + z^2/2R^2)$. In the approximation of equal mass in the inner and outer face of the torus, simultaneous tilt of one ring upwards and the other ring downwards is associated with the potential energy

$$U_g(\theta) \simeq -\frac{M_T M_H}{R} \left(1 - \frac{1}{4} \tan^2(\theta/2) \right), \quad (5)$$

with $\tan(\theta/2) = z/R$, where we averaged over all segments of a ring. Note that $U_g(\theta)$ has period π and is minimal when $\theta = 0$. Stability is accomplished provided that the total potential energy $U(\theta) = U_\mu(\theta) + U_g(\theta)$ satisfies

$$\frac{d^2 U}{d\theta^2} > 0. \quad (6)$$

The potential $U(\theta)$ is shown in Fig. 7, which shows the bifurcation at $b = 1/12$ of the stable equilibrium $\theta = 0$ into an unstable equilibrium with the appearance of two neighboring stable equilibria at non-zero angles. The bifurcation point is therefore second order. Nevertheless, the torus may become nonlinearly unstable at large angles ($b \gg b^*$). We therefore consider below the physical parameters at this bifurcation point.

For two rings of radii R_\pm with $(R_+ - R_-)/(R_+ + R_-) = O(1)$, we have $U_\mu \simeq \frac{1}{2} B^2 R^3 \cos \theta$, so that (6) gives $B_c^2 M_H^2 = (1/4)(M_H/R)^4 (M_T/M_H)$, or

$$B_c \simeq 10^{16} \text{G} \left(\frac{7M_\odot}{M_H} \right) \left(\frac{6M_H}{R} \right)^2 \left(\frac{M_T}{0.03M_H} \right)^{1/2}. \quad (7)$$

The critical value of the ratio of poloidal magnetic energy ($\mathcal{E}_B = f_B B^2 R^3/6$) to kinetic energy ($M_T M_H/2R$) in the torus becomes

$$\left. \frac{\mathcal{E}_B}{\mathcal{E}_k} \right|_c = \frac{f_B}{12}, \quad (8)$$

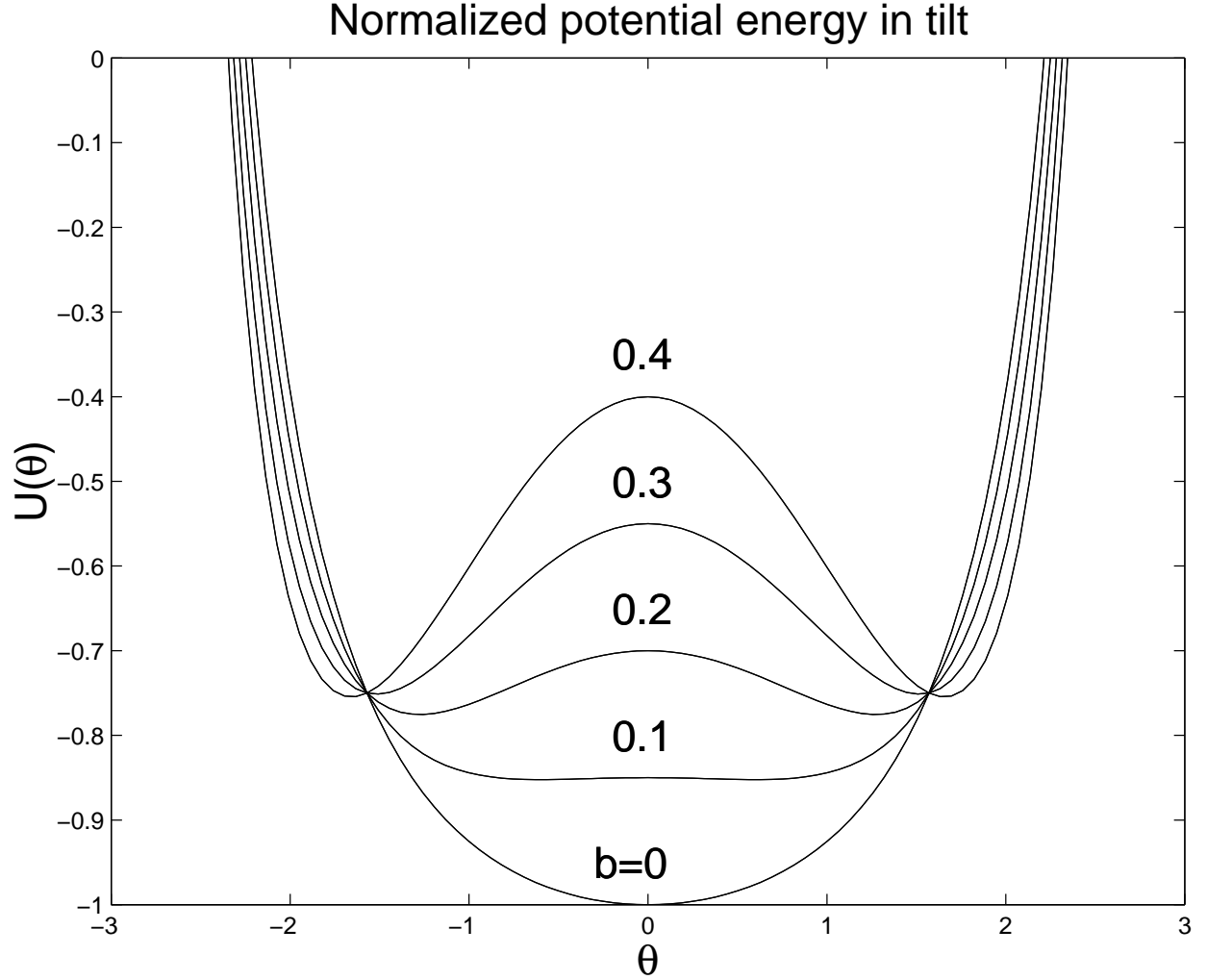


Fig. 7.— The potential energy associated with a poloidal tilt angle θ between the inner and the outer rings is the sum of a magnetic moment-magnetic moment interaction plus a tidal interaction with the central potential well of the black hole. It is shown for various normalized magnetic field-energies $b = \mathcal{E}_B/\mathcal{E}_k$. The equilibrium $\theta = 0$ becomes unstable when $d^2U(\theta)/d\theta^2 < 0$, corresponding to a bifurcation into two stable branches of non-zero angles beyond $b > 1/12$.

where f_B denotes a factor of order unity, representing the volume of the inner torus magnetosphere as a fraction of $4\pi R^3/3$. We emphasize that the limit (8) is fundamental, independent of the mass of the black hole, and the mass and radius of the torus. This result can equivalently be attributed to stable balance of Lorentz forces against tidal forces, preventing a small misalignment to cause a tilt.

The poloidal magnetic field introduces an anisotropic pressure tensor. At the critical magnetic field-strength (7), pressure components in the equatorial plane are predominantly magnetic rather than thermal at MeV temperatures. The poloidal pressure components (along the magnetic field-lines) are thermal pressures. In equilibrium, these poloidal pressure components are unaffected by poloidal tidal forces if the poloidal flux-surfaces assume a spherical shape inside of the torus.

The magnetic field may be generated in response to the power received from the black hole. If so, then $d\mathcal{E}_B/dt \leq L_H$, where (Thorne, et al. 1986; van Putten 1999)

$$L_H \simeq \frac{1}{32} \eta B^2 M_H^2, \quad (9)$$

denotes the black hole-luminosity expressed in terms of a fraction $\eta = \Omega_T/\Omega_H$ of the angular velocity of the torus to that of the black hole. The discrepancy $L_H - d\mathcal{E}_B/dt$ is carried away in the various channels as described in the suspended accretion state, and will be zero in equilibrium. This gives rise to a minimum e-folding time

$$\tau_B = \frac{8}{3} \eta^{-1} \left(\frac{R}{M_H} \right)^2 R = 0.2 \text{s} \left(\frac{\eta}{0.1} \right)^{-1} \left(\frac{R}{6M_H} \right)^3 \left(\frac{M_H}{7M_\odot} \right). \quad (10)$$

A critical magnetic field of $B_c \simeq 10^{16} \text{G}$ is hereby reached on a time-scale of at least a few seconds. The suspended accretion state may hereby be intermittent on an intermediate time-scale of seconds, associated with magnetic field build-up powered by the rotational energy of the black hole.

Most of the rotational energy is dissipated in the horizon, creating entropy S for a black hole temperature T_H at a maximal rate $T_H \dot{S} \simeq B^2 M^2 / 32$ (Thorne, et al. 1986). The lifetime of rapid rotation of the black hole becomes effectively the timescale of dissipation of black hole-spin energy $E_{rot} \simeq M_H/3$ in the horizon, i.e.:

$$T \simeq \frac{E_{rot}}{T_H \dot{S}} \geq 40 \text{ s} \left(\frac{M_H}{7M_\odot} \right) \left(\frac{R}{6M_H} \right)^4 \left(\frac{0.03M_H}{M_T} \right), \quad (11)$$

where eq. (7) has been employed.

The suspended accretion state, conceivably intermittent on a timescale (10), lasts for a duration similar to (11) until the ISCO reaches the torus or until $\Omega_H \simeq \Omega_T$, whichever comes first.

3.2. A magnetic buckling instability

We partition the magnetization of the torus into N equidistant fluid elements with dipole moments, $\mu_i = \mu/N = (1/2)BR^3/N$. We consider the vertical degree of freedom, of fluid elements which move to a height z above the equatorial plane. By conservation of angular momentum, this motion is restricted to a cylinder of constant radius. Their position vectors in and off the equatorial plane will be denoted by

$$\mathbf{r}_i^e = (R \cos \phi_i, R \sin \phi_i, 0), \quad \mathbf{r}_i = (R \cos \phi_i, R \sin \phi_i, z_i), \quad \phi_i = 2\pi i/N. \quad (12)$$

A fluid element i assumes an energy which consists of magnetic moment-magnetic moment interactions and the tidal interaction with the central potential well. The total potential energy of the i -th fluid element is given by

$$U_i = -\frac{\mu_i B'}{N} \sum_{j \neq i} \frac{|\mathbf{r}_i^e - \mathbf{r}_j^e|^3}{|\mathbf{r}_i - \mathbf{r}_j|^3} \cos \theta_{ij} + U_g(\theta_i), \quad (13)$$

where $B' = B/N^*$ denotes the magnetic field-strength of a magnetic dipole at distance $d = 2\pi R/N$, θ_{ij} denotes the angle between the i -th magnetic moment and the local magnetic field of the j -th magnetic moment, and $U_{gi} = -(M_T M_H / RN)(1 - z_i^2 / 2R^2)$ the tidal interaction of the i -th fluid element with the black hole. Here, N^* is a factor of order N which satisfies the normalization condition $\sum_i U_i = -\mu B$ (in equilibrium). Upon neglecting azimuthal curvature in the interaction of neighboring magnetic moments, we have a magnetic moment-magnetic moment interaction

$$\mu_i B' \frac{|\mathbf{r}_i^e - \mathbf{r}_j^e|^3}{|\mathbf{r}_i - \mathbf{r}_j|^3} \cos \theta_{ij} \simeq \frac{\mu_i B'}{|i - j|^3} \left(1 - \left[1 + \frac{3}{2|i - j|^2} \right] \alpha_{ij}^2 \right), \quad (14)$$

where $\alpha_{ij} = (z_i - z_j)/d$,

$$\cos \theta_{ij} = -\sqrt{(1 - \alpha_{ij}^2)/(1 + \alpha_{ij}^2)} \simeq -(1 - \alpha_{ij}^2), \quad (15)$$

and $|\mathbf{r}_i - \mathbf{r}_j| \simeq |i - j|d(1 + \alpha_{ij}^2/2|i - j|^2)$.

We shall use the small amplitude approximation, whereby $z_i/R = \tan \theta_i \simeq \theta_i$. We study the stability of this configuration, to derive an upper limit for the magnetic field-strength. An upper limit obtains by taking into account only interactions between neighboring magnetic moments. (The sharpest limit obtains by taking into account interactions between one magnetic moment and all its neighbors.) Thus, we have $N^* = 2N$ and consider the total potential energy

$$U_i = \frac{\mu_i B'}{N} \sum_{|i-j|=1} \left(1 - \frac{5}{2} \alpha_{ij}^2 \right) + U_g(\theta_i), \quad (16)$$

where $\alpha_{ij} = N(\theta_i - \theta_j)/2\pi$. The Euler-Lagrange equations of motion are

$$\frac{M_T R}{N} \ddot{\theta}_i + \frac{\partial U_i}{R \partial \theta_i} = 0. \quad (17)$$

This defines the system of equations for the vector $\mathbf{x} = (\theta_1, \theta_2, \dots, \theta_N)$ given by

$$\frac{M_T R}{N} \ddot{\mathbf{x}} + \frac{M_T M_H}{N R^2} \mathbf{x} = \frac{5\mu B}{2N} \begin{pmatrix} 2 & -1 & 0 & \cdots & 0 & -1 \\ -1 & 2 & -1 & \cdots & 0 & 0 \\ & & \cdots & & & \\ -1 & 0 & \cdots & 0 & -1 & 2 \end{pmatrix} \mathbf{x} \quad (18)$$

The least stable eigenvector is $\mathbf{x} = (1, -1, 1, \dots, -1)$ (for N even), for which the critical value of the magnetic field is

$$B_c^2 M_H^2 = \frac{1}{5} \left(\frac{M_T}{M_H} \right) \left(\frac{M_H}{R} \right)^4. \quad (19)$$

This condition is very similar to (7), and gives a commensurable estimate

$$\left. \frac{\mathcal{E}_B}{\mathcal{E}_k} \right|_c = \frac{1}{15} \quad (20)$$

and lifetime of rapid spin of the black hole.

We propose to identify the redshift-corrected durations of long gamma-ray bursts and their contemporaneous emissions in gravitational radiation (Fig. 8) with this new secular time-scale (11) of tens of seconds, set by the stability-limited energy of the poloidal magnetic field supported by the torus.

A high-order approach can be envisioned, in which the inner and outer face of the torus are each partitioned by a ring of magnetized fluid elements. This is of potential interest in studying instabilities in response to shear, in view of the relative angular velocity $\Omega_+ - \Omega_- > 0$. Magnetic coupling between the two faces of the torus through aforementioned tilt or buckling modes inevitably leads to transport of energy and angular momentum from the inner face to the outer face of the torus by the Rayleigh criterion. A detailed discussion of this instability falls outside the scope of the present paper.

4. Multipole mass moments in a torus in suspended accretion

As explained in §2, the torus is sandwiched between a magnetic wall around the black hole and an outer torus magnetosphere. It is hereby subject to competing torques on the

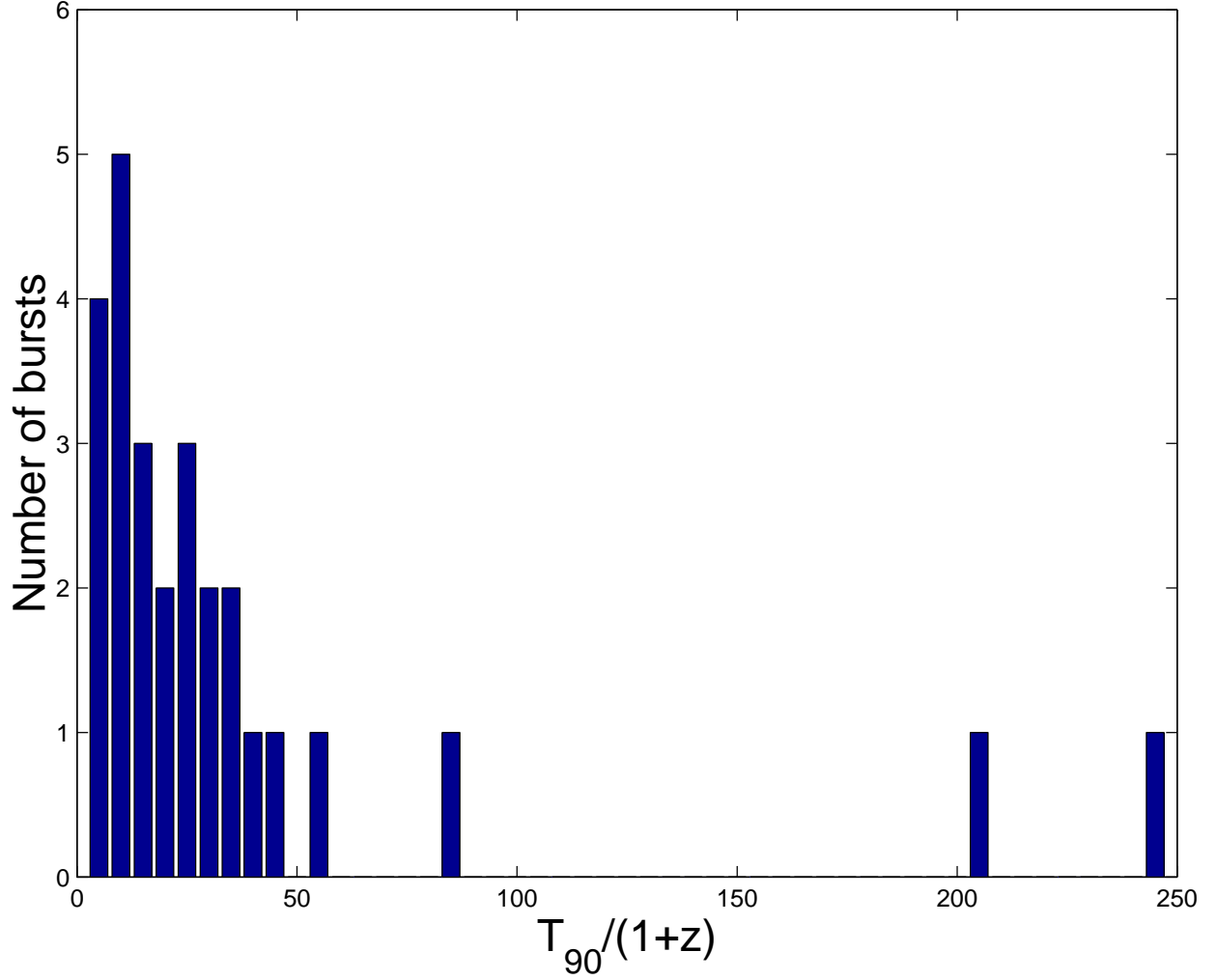


Fig. 8.— Shown is the histogram of redshift corrected durations of 27 long bursts with individually determined redshifts from their afterglow emissions. We identify these long durations with the lifetime of rapid spin of a Kerr black hole in a state of suspended accretion. These durations are effectively defined by the rate of dissipation of black hole-spin energy in the horizon, which is subject to a new magnetic stability criterion for the torus. (Reprinted from M.H.P.M. van Putten, 2002, ApJ, 575, L71).

inner and the outer face, which introduces heating and, possibly, turbulent magnetohydrodynamical flow. This is stimulated by a finite number of multipole mass moments produced by the Papaloizou-Pringle instability in a torus of finite width. The net rate of dissipation can be calculated in the suspended accretion state, from balance of energy and angular momentum in combination with emissions in gravitational radiation and magnetic winds.

A torus tends to develop instabilities in response to shear, which can be studied analytically in the approximation of incompressible fluid about an unperturbed angular velocity

$$\Omega = \Omega_a \left(\frac{a}{r} \right)^q, \quad (21)$$

where $q \geq 3/2$ denotes the rotation index and $a = (R_+ + R_-)/2$ denotes the major radius of the torus. In the inviscid limit, irrotational modes in response to initially irrotational perturbations to the underlying flow (vortical if $q \neq 2$) shows the Papaloizou-Pringle instability (Papaloizou & Pringle 1984) to also operate in wide tori (van Putten 2002a). The neutral stability curves of the resulting buckling modes are described by a critical rotation index $q_c = q_c(\delta, m)$ as a function of the slenderness parameter $\delta = b/2a$, where $b = (R_- - R_+)/2$ denotes the minor radius of the torus and $a = (R_- + R_+)/2$ the mean radius (Fig. 9), where m denotes the azimuthal wave-number.

It will be appreciated that the torus is $m = 0$ stable for perturbations of its radius (in the mean). This is due to the frozen-in condition of magnetic flux-surfaces. In terms of angular momentum transport, the horizon magnetic flux $\propto (M/a)^2$ hereby defines a black hole-to-torus coupling which is dominant over the coupling $\propto \Omega_T \simeq M/a^{3/2}$ of the torus to infinity.

Quadratic fits to the stability curves are

$$q_c(\delta, m) = \begin{cases} 0.10(\delta/0.1)^2 + 1.73 & (m = 2) \\ 0.26(\delta/0.1)^2 + 1.73 & (m = 3) \\ 0.50(\delta/0.1)^2 + 1.73 & (m = 4) \\ 0.80(\delta/0.1)^2 + 1.73 & (m = 5) \\ 0.034m^2(\delta/0.1)^2 + 1.73 & (m > 5) \end{cases} \quad (22)$$

Instability sets in above these curves, stability below. For $m = 2$, the critical value $q_c = 2$ obtains for $\delta = 0.16$, associated with the Rayleigh stability criterion for the azimuthally symmetric wave mode $m = 0$. For large m , we use the numerical result of critical values $\delta = 0.28/m$ for $q = 2$.

The central pressure of the torus is produced by differential rotation, due to a state of super-keplerian motion of the inner face and a state of sub-keplerian motion of the outer face. This pressure is balanced by both magnetic and thermal pressure at MeV temperatures,

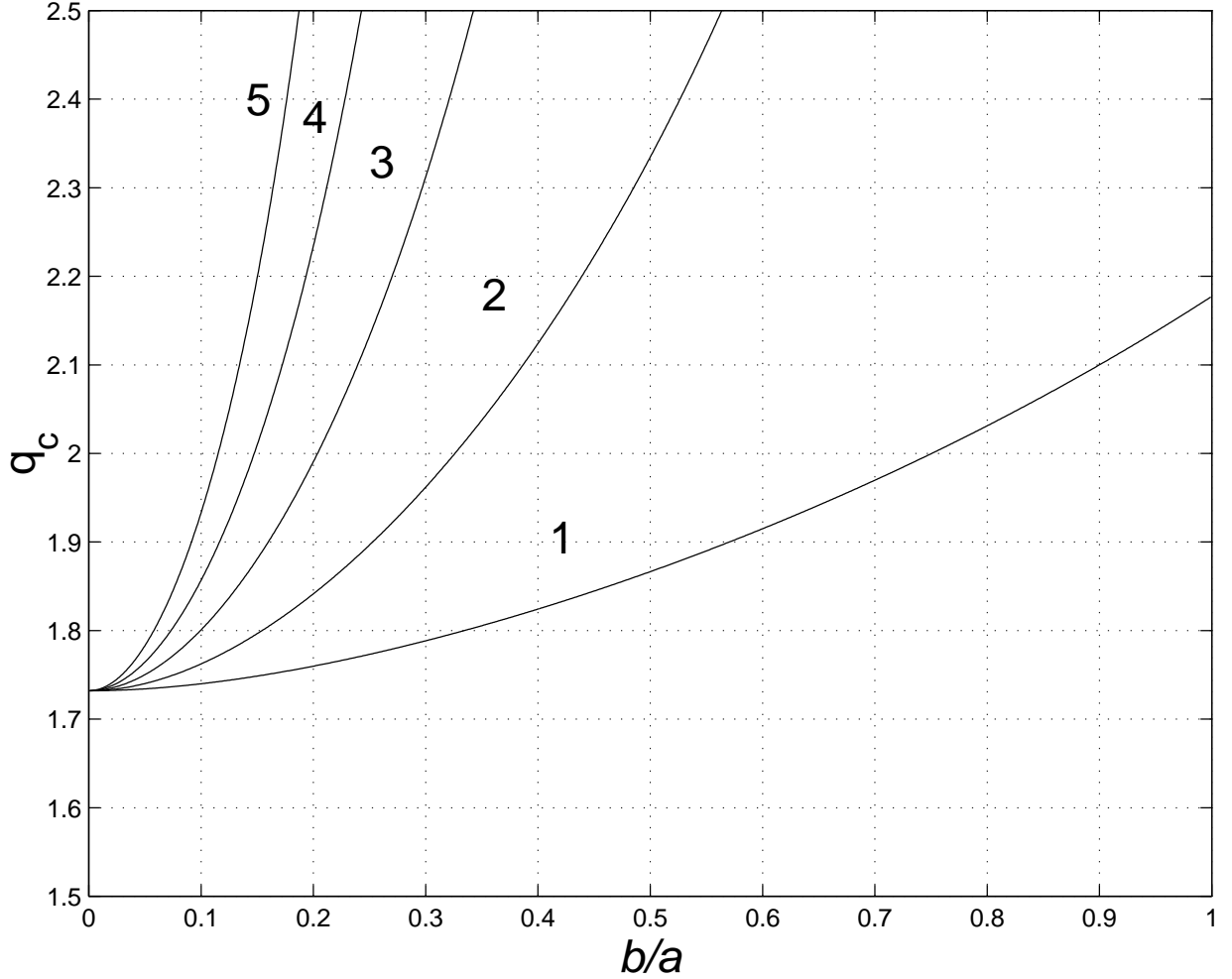


Fig. 9.— Diagram showing the neutral stability curves for the non-axisymmetric buckling modes in a torus of incompressible fluid, as an extension of the Papaloizou-Pringle instabilities to finite slenderness ratios $\delta = b/2a > 0$, where b and a denote the minor and major radius of the torus, respectively. Curves of critical rotation index q_c are labeled with azimuthal quantum numbers $m = 1, 2, \dots$, where instability sets in above and stability sets in below. The central pressure produced by super- and subkeplerian motions of the inner and outer face of the torus is balanced by magnetic and thermal pressure at MeV temperatures. At finite slenderness $0 < b/a \ll 1$, this produces instability to a finite number of Papaloizou-Pringle modes (Reprinted from M.H.P.M. van Putten, ApJ, 575, L71).

which gives rise to finite slenderness $\delta > 0$ and hence instability to a finite number of Papaloizou-Pringle modes. Thermal pressure alone gives the estimate (adapted from van Putten (2002a))

$$q \simeq 1.5 + 0.2 \left(\frac{0.1}{\delta} \right)^2 \left(\frac{kT}{2\text{MeV}} \right). \quad (23)$$

Magnetic pressure enhances this estimate to larger values of q . This shows that a torus of finite slenderness ($\delta < 0.1$) and a radius around $5M$ is unstable ($q > \sqrt{3}$) to the formation of a finite number of multipole mass moments by the Papaloizou-Pringle instability. A torus with multiple mass moments potentially defines a gravitational wave-spectrum consisting of several lines.

5. Energy emissions by the torus

The suspended accretion state in the case of a symmetric flux-distribution, given by equal fractions of open magnetic flux on the inner and the outer face, gives rise to remarkably simple expressions for the predicted energy output in the relevant channels. To leading order the angular velocities of the inner and outer faces are given in terms of the mean angular velocity of the torus, $\Omega_T = (\Omega_- + \Omega_+)/2$, and the slenderness ratio δ , as $\Omega_{\pm} = \Omega_T(1 \pm \delta)$. Equation 2 implies that for a small slenderness ratio, $L_- \simeq \eta L_+$, where $\eta = \Omega_T/\Omega_H$ denotes the ratio of the angular velocity of the torus to that of the black hole. In the limit of strong magnetohydrodynamical viscosity and small slenderness ratio we then have the asymptotic results (van Putten 2002b)

$$E_{gw}/E_{rot} \sim \eta, \quad E_w/E_{rot} \sim \eta^2, \quad E_d/E_{rot} \sim \eta\delta, \quad (24)$$

where E_{gw} , E_w , E_d are defined below.

Gravitational radiation. The major energy output from the torus is in gravitational radiation,

$$E_{gw} = 6 \times 10^{53} \text{erg} \left(\frac{\eta}{0.1} \right) \left(\frac{M_H}{10M_{\odot}} \right). \quad (25)$$

A quadrupole buckling mode radiates gravitational waves at close to twice the angular frequency of torus (van Putten 2002a). These emissions are relatively powerful, representing about 10% of the rotational energy of the black hole for the lifetime of the system. The associated mass inhomogeneity δM_T in the torus assumes a value commensurate with the inferred luminosity in gravitational radiation. For quadrupole emissions, we have

$L_{GW} \simeq (32/5)(M_H/R)^5(\delta M_T/M_H)^2$, where $\omega \simeq M_H^{1/2}R^{-3/2}$ denotes the orbital angular frequency at a radius R , assuming approximately circular motion. The estimated gravitational wave-luminosity is hereby produced by $\delta M_T \simeq 0.5\%M_H(R/5M_H)^{7/4}$. This corresponds to a mass inhomogeneity of 20% for a torus $M_T = 0.2M_\odot$ around a black hole of mass $M_H = 7M_\odot$.

Torus winds. The energy output in torus winds is a factor η less than that in gravitational radiation, or

$$E_w = 6 \times 10^{52} \text{erg} \left(\frac{\eta}{0.1} \right)^2 \left(\frac{M}{10M_\odot} \right). \quad (26)$$

These powerful torus winds may produce hypernova remnants in the host environment, e.g., a shell associated with a molecular cloud. They may be baryon loaded and deposit some torus matter onto the companion star as in the Brown et al. (2000) association of hypernovae to soft X-ray transients, and they may be important in collimating baryon poor jets produced by the black hole. Finally, these winds are potentially relevant in r-processes (Levinson & Eichler 1993). This suggests considering observational methods to determine E_w , from which to determine the system parameter η , and hence the frequency of gravitational radiation. Of potential interest are model dependent estimates of E_w from their role in collimating outflows, and calorimetry on hypernova remnants. The first can be pursued using existing data on GRB beaming angles, which suggests a value of $\eta \simeq 0.1$. The second method is potentially more reliable, but awaits further study on the identification and observational aspects of hypernova remnants.

Torus temperature. The energy output in thermal and neutrino emissions is a factor δ less than that in gravitational radiation, or

$$E_d = 10^{53} \text{erg} \left(\frac{\eta}{0.1} \right) \left(\frac{\delta}{0.15} \right) \left(\frac{M_H}{10M_\odot} \right). \quad (27)$$

Here, we refer to a fiducial value of $\eta \simeq 0.1$ as before, as well as a value $\delta \simeq 0.15$ or less. The latter is suggested by quadrupole radiation of gravitational waves which requires $\delta \leq 0.16$ at the threshold of Rayleigh stability, according to (22). This dissipation rate corresponds to a temperature of a few MeV (see eq. [29] below), which thereby produces baryonic winds. The torus winds considered here, therefore, are baryon rich.

6. Pressure driven mass ejection from the torus

It has been argued in §5 above that a fraction E_d/E_{rot} of the black hole-spin energy is dissipated in the torus, thereby heating it to a temperature in excess of a few MeV. This drives a powerful wind by the pressure gradients in the surface layers of the torus. The resulting mass ejection opens magnetic field lines that pass through the outer Alfvén point, and folds some of those in the outer layers of the inner magnetosphere. This creates a change in poloidal topology in the form of a coaxial structure of open flux tubes with opposite magnetic orientation (towards infinity). Because the torus is rotating and magnetized, the ejection of the wind is partially anisotropic. Specifically, mass flux is generally suppressed along magnetic field lines that are inclined toward the rotation axis, and enhanced along field lines that are strongly inclined away from the axis (Blandford & Payne 1982; Romanova et al. 1997), owing to centrifugal forces. The details of the outflow depend on the heating and cooling rate of the corona, and on its structure, and analysis thereof is beyond the scope of the present discussion. In what follows, we provide a rough estimate for the mass flux expelled in the vertical direction, speculate on the implications for opening of magnetic field lines, and discuss the consequences of mass ejection in the equatorial plane for the energy extraction process.

6.1. An estimate of the vertical mass flux

A torus having a temperature in excess of a few MeV, and an average density $\tilde{\rho}_b \sim 10^{11}(M_T/0.1M_\odot)/V_{21}$ gr cm⁻³, where $V = 10^{21}V_{21}$ cm³ is the volume of the torus, cools predominantly by neutrino emission through electron and positron capture on nucleons. The cooling rate is given by (e.g., Bethe & Wilson 1985)

$$\epsilon_{\text{cap}} \simeq 10^{29} \tilde{\rho}_{b11} T_{10}^6 \text{ ergs s}^{-1} \text{ cm}^{-3}, \quad (28)$$

where T_{10} is the average temperature in units of 10^{10} K. For a total energy dissipation rate of $L = 10^{52}L_{52}$ ergs, we then find an average temperature of

$$T_{10} \simeq 2L_{52}^{1/6} (M_T/0.1M_\odot)^{-1/6}. \quad (29)$$

As will be shown below, the mass flux from the surface depends on the temperature profile in the neighborhood of the flow critical point, where the density is well below the average. The latter can be determined in principle by equating the local heating and cooling rates, provided that adiabatic cooling there can be neglected (which we find to be justified only if the temperature exceeds $\sim 2 \times 10^{10}$ K). While the fraction of the black hole spin-energy dissipated in the surface layers is not well constrained, a fraction of the energy of

neutrinos escaping from the dense regions – well beneath the surface – will be deposited in the surface layers of the torus. The dominant absorption processes for the latter are neutrino capture on neutrons and protons and pair neutrino annihilation into electron-positron pair. These processes typically dominate at lower densities and higher temperatures. In spherical geometry, the heating rate is dominated by neutrino annihilation at densities below $\rho = 6 \times 10^7 (L_{52}/R_{\nu 6}^2)^{1/2} (R_{\nu}/r)^6 \text{ gr cm}^{-3}$, where $R_{\nu} = 10^6 R_{\nu 6} \text{ cm}$ is the radius of the neutrino production region (Levinson & Eichler 1993). The cooling rate due to electron-positron annihilation into neutrinos depends sensitively on temperature ($\epsilon_{\nu\bar{\nu}} \propto T^9$), and dominates over the energy loss rate by electron and positron capture on nucleons at densities below $\rho = 5 \times 10^6 T_{10}^3 \text{ gr cm}^{-3}$ (Levinson & Eichler 1993). Taking into account both processes, we find, up to a geometrical factor, that the critical point (see eq. [37] below) will be maintained roughly at the average temperature given by eq. (29).

Now, the torus material should be a mixture of baryons and a light fluid (photons and electron-positron pairs in equilibrium). The light and baryonic fluids will be tightly coupled, owing to the large Thomson depth. Deep beneath its surface, the torus is in a hydrostatic equilibrium where the vertical gravitational force exerted on it by the black hole is supported by the baryon pressure $p_b = n_b kT$. At baryon densities

$$\rho_b < \frac{p_l m_p}{kT} \simeq 10^{11} T_{10}^3 \text{ gr cm}^{-3}, \quad (30)$$

the light fluid pressure,

$$p_l = 2 \times 10^{25} T_{10}^4 \text{ dyn cm}^{-2}, \quad (31)$$

exceeds the pressure contributed by the baryons. At sufficiently shallow layers, the light fluid pressure gradient overcomes the vertical gravitational force, and the matter starts to accelerate. The transonic flow should pass through a critical point. To estimate the mass flux we calculate below the wind density and velocity at the critical point.

To simplify the analysis we neglect general relativistic effects. Since we are merely interested in an estimate for the mass loss rate, we need only to consider the properties of the flow in the neighborhood of the critical point. Since the latter is located well within the light cylinder, we neglect rotation of the torus and the toroidal magnetic field. (This is not valid in general, but is used only in regards to mass ejection from the upper and lower faces of the torus.) Below, we find that the flow becomes mildly relativistic at the critical point. The MHD limit applies, in view of high electric conductivity in the coupled light plus baryonic fluids, whereby the streamlines of the flow are along magnetic flux-surfaces. Baryon number conservation, viz., $\nabla(n_b \mathbf{u}_p) = 0$, where \mathbf{u}_p denotes the poloidal 4-velocity and n_b the baryon number density, and Maxwell's equation, $\nabla \times \mathbf{E} = 0$, imply that the flux of baryons per unit magnetic flux is conserved:

$$(n_b u_p / B_p)' = 0. \quad (32)$$

Here B_p is the poloidal magnetic field, and $'$ denotes derivative along streamlines (i.e., $\mathbf{u}_p \cdot \nabla$). In the limit of weak gravitational field, the projection of the momentum equation, $T^{i\nu}_{;\nu} = 0$, on the poloidal direction, and the use of eq. (32) gives (Camenzind 1986; Takahashi et al. 1990)

$$u_p(1 - M^{-2})u'_p = -\frac{\gamma^2}{1 - a_s^2}[a_s^2(\ln B_p)' + \psi'], \quad (33)$$

where $\gamma^2 = 1 + u_p^2$ is the Lorentz factor of the flow, $\psi = GM_H/rc^2$ is the gravitational potential,

$$a_s = \left(\frac{4p_l}{12p_l + 3\rho_b c^2} \right)^{1/2}, \quad (34)$$

is the sound speed of the mixed fluid (measured in units of c), and $M = u_p/c_s$, with $c_s = a_s/\sqrt{1 - a_s^2}$ being the sound four speed, is the corresponding Mach number. It is seen that the flow has a critical point at $M = 1$. We note that under the assumption made above, that the toroidal magnetic field can be ignored, this critical point coincides essentially with the fast magnetosonic point. We now suppose that the flow passes through this critical point, which should be true in the case of a wind expelled along open magnetic field lines. There the right-hand side of eq. (33) must also vanish. The latter condition can be solved to yield the sound speed at the critical point:

$$a_{sc}^2 = -\frac{\psi'}{(\ln B_p)'} = \frac{GM_H}{c^2 r_c^2} \frac{r'}{(\ln B_p)'}, \quad (35)$$

where $r_c \sim a$ is the radius of the critical point. It is seen that the critical sound speed depends on the geometry of the field lines in the vicinity of the critical point. To obtain an order of magnitude estimate, let us assume that $r' \sim \xi_c/r_c$, and $(\ln B_p)' \sim \xi_c^{-1}$, where $\xi_c < r_c$ denotes the distance from the torus midplane to the critical point along streamlines. Then

$$a_{sc} \simeq \left(\frac{GM_H}{c^2 r_c} \right)^{1/2} \left(\frac{\xi_c}{r_c} \right) = 0.3 \left(\frac{M_H}{10M_\odot} \right)^{1/2} r_{c7}^{-1/2} (\xi_c/r_c). \quad (36)$$

The critical density can be obtained now by employing eqs. (29), (34) and (36):

$$\rho_{bc} = \frac{p_l (4 - 12a_{sc}^2)}{c^2 a_{sc}^2} \simeq 1 \times 10^7 \left(\frac{M_H}{10M_\odot} \right)^{-1} \left(\frac{M_T}{0.1M_\odot} \right)^{-2/3} r_{c7} (\xi_c/r_c)^{-2} L_{52}^{2/3} \text{ gr cm}^{-3}. \quad (37)$$

The associated mass flux is given by

$$\rho_{bc} c_s \simeq 1 \times 10^{17} \left(\frac{M_H}{10M_\odot} \right)^{-1/2} \left(\frac{M_T}{0.1M_\odot} \right)^{-2/3} r_{c7}^{1/2} (\xi_c/r_c)^{-1} L_{52}^{2/3} \text{ gr cm}^{-2} \text{ s}^{-1}, \quad (38)$$

which corresponds to a mass loss rate of $\dot{M} \simeq 1 \times 10^{30} \text{ gr s}^{-1}$ for a surface area of $A = 0.1a^2 = 10^{13}a_7^2 \text{ cm}^2$. We conclude that during the $\sim 30 \text{ s}$ suspended accretion state the torus will be partially evaporated.

Finally, we note that the Alfven Mach number at the critical point is

$$M_A = \left(\frac{16\pi p_l}{3B_p^2} \right)^{1/2} \simeq 0.07(M_T/0.1M_\odot)^{-1/3} L_{52}^{1/3} B_{p15}^{-1}. \quad (39)$$

We thus conclude that, for our choice of torus parameters, the outflow is sub-Alfvenic (but not highly so) at the critical point.

6.2. Creation of open field-lines

The ejection of matter from the hot torus corona will result in the opening of some magnetic field lines in the outer layers of the inner torus magnetosphere (Fig. 10). By eq. (39), plasma which streams along field lines that extend to large distances quickly reach the Alfven point. These field lines become nearly radial several scale height above the torus, forming an open flux tube. For field lines that converge toward the rotation axis of the black hole the above analysis is probably inapplicable, as the centrifugal force cannot be ignored. Large pressure gradients in the corona would tend to push matter along some of the magnetic field lines in the outer layers of the inner torus magnetosphere. A combination of buoyancy and centrifugal forces may subsequently give rise to a twist of these field lines, some of which may ultimately fold and open, to form a region of oppositely directed magnetic field lines. Field lines thus created near the axis constitute the inner flux tube that extends from the horizon to infinity; those anchored to the torus now extend to infinity and constitute an outer flux tube. The inner and outer flux tubes have opposite magnetic orientation and are separated by a charge and current sheet, whenever the outer tube carries a (super-Alfvénic) wind to infinity. Reconnection may occur in the boundary layer, which is of interest in the rearrangement of the magnetosphere near the axis. This coaxial structure of open flux tubes is discussed in greater detail in the next section.

A crucial issue is the opening angle of the inner flux tube on the horizon of the black hole, as it forms an artery for its spin-energy. We consider it probable that the opening angle depends only on the overall geometry of the system (black hole mass and radius of the torus). A universal half-opening angle on the horizon gives rise to a standard fraction of black hole-spin energy released through the inner flux-tube.

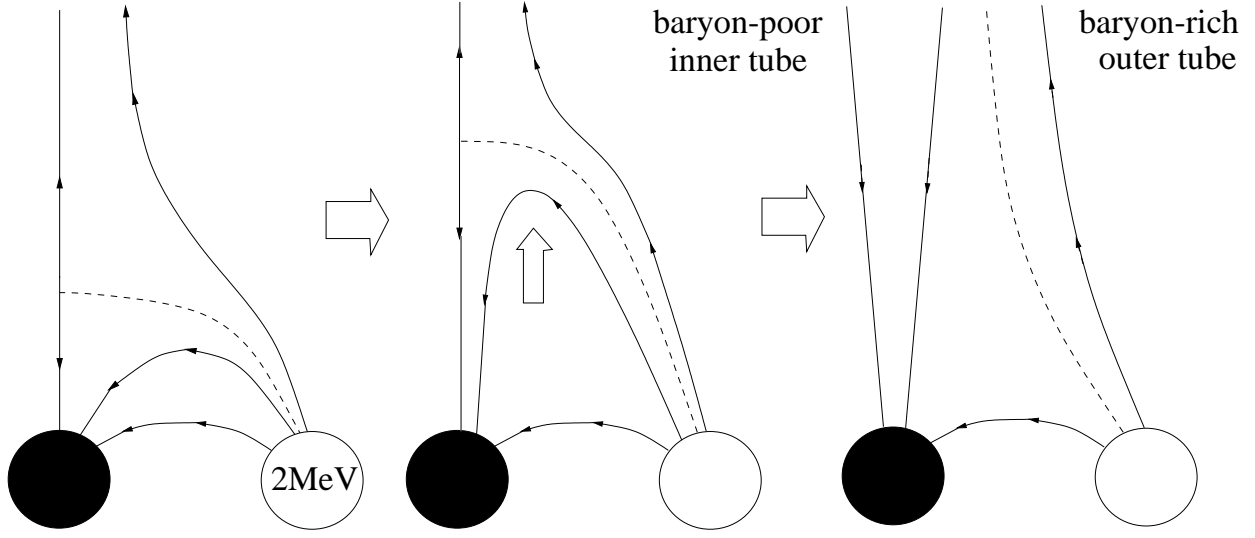


Fig. 10.— The MeV temperature of the torus produces powerful torus winds. We propose that these winds open an outer layer of flux-surfaces, supported by the inner face of the torus. This is schematically indicated by a stretch, fold and cut of the separatrix (dashed lines) between the inner and outer flux-surfaces. This leaves an open, inner tube of magnetic flux supported by the black hole and an open, outer flux tube of magnetic flux supported by the inner face of the torus. The inner tube is baryon-poor; the outer tube is baryon-rich. The lower/upper sections of this structure contain parallel/antiparallel orientation of the poloidal magnetic field. The inner tube serves as an artery for baryon-poor outflow from the black hole.

6.3. Implications for energy extraction from the black hole

The rate at which the torus catalyzes black hole spin-energy has been calculated in §5 under the assumption that the torus magnetosphere is force-free. However, ejection of appreciable mass flux along magnetic field lines that thread the horizon may alter the extraction process. Detailed study of ideal MHD flow in Kerr geometry is provided by Takahashi et al. (1990), and Hirotani et al. (1992). They analyze the conditions under which energy extraction occurs in a flow that starts with a zero poloidal velocity at the plasma source and is pulled inward by the black hole. They show that the MHD flow can carry a negative energy flux into the horizon (which is equivalent to the condition that the energy given by eq. [A9] is negative), provided that i) the angular velocity of magnetic field lines lies in the range $0 < \Omega_F < \Omega_H$, where Ω_H is the angular velocity of the black hole (which is identical to the condition found by Blandford & Znajek (1977)), and ii) the Alfvén point is located inside the ergosphere, which implies that inflow of negative electromagnetic energy exceeds inflow of positive kinetic energy. The latter condition restricts the mass flux expelled along field lines connecting the torus and the horizon. The vertical mass flux estimated above assumes maximum extraction efficiency. We argue that inward mass ejection in the equatorial plane may be suppressed by the centrifugal barrier. The details are complicated by virtue of general relativistic effects. Whether this is sufficient to allow energy extraction is not clear at present. If not, it would mean that the rate at which the spin down energy of the hole is dissipated in the torus and, hence, its temperature, must be regulated by mass ejection.

7. Structure of the inner flux-tube

In the preceding section we argued that mass ejection from the torus opens magnetic field lines on the outer layers of the inner torus magnetosphere. This creates an open magnetic flux tube that extends from the horizon to infinity, surrounded by an outer flux-tube that is anchored to the torus. The upper sections of this structure results from a fold, stretch and cut in poloidal topology, whereby the inner and outer tubes assume mutually antiparallel poloidal magnetic field. The lower section remains unfolded, leaving parallel poloidal magnetic fields in the inner and outer flux-tubes (see Figs. 4, 10). This additional structure was not analyzed in (van Putten & Levinson 2002). In what follows, we describe the structure of the inner tube in some detail.

7.1. Asymptotic boundary conditions on the horizon and at infinity

The inner flux tube satisfies slip/slip boundary conditions both on the horizon and at infinity. It is well known that in the limit of infinite conductivity, every magnetic surface must rotate rigidly (although the angular velocity of different flux surfaces should not be the same). Finite resistivity effects, however, may give rise to a differential rotation along magnetic flux tubes (implying $\mathbf{E} \cdot \mathbf{B} \neq 0$). To make our analysis general, we shall allow for such a differential rotation, and denote the angular velocities of a given flux surface on the horizon and at infinity by Ω_{F+} and Ω_{F-} , respectively.

As stated above, we anticipate the horizon half-opening angle θ_H of the inner flux tube to be sufficiently small so that the small-angle approximation applies in solving Maxwell's equations. From equation (A20) we obtain

$$2\pi \int j^r \sqrt{-g} d\theta = \frac{\Delta}{2\rho^2} \sin \theta F_{r\theta} \equiv \frac{1}{2} B_T. \quad (40)$$

It can be readily shown (e.g., Blandford & Znajek (1977)) that in the force-free limit, viz., $F_{\mu\nu} j^\nu = 0$, the Boyer-Lindquist toroidal magnetic field, B_T , is conserved along magnetic flux surfaces $\Psi(r, \theta)$, and that the current contained within a magnetic flux surface is given exactly by eq. (40), viz., $I(\Psi) = (1/2)B_T$ and, hence, is also conserved. Current conservation along streamlines is not guaranteed in general, however, even in the limit of infinite conductivity, since inertial effects may give rise to cross field currents. At any rate, beyond the fast magnetosonic point of the inflow (outflow), the poloidal current becomes radial asymptotically, as it is carried purely by the inflowing (outflowing) Goldreich-Julian charges (see below). By employing the asymptotically frozen-in condition on the horizon, $F_{r\theta} = (\Sigma/\Delta)(\Omega_H - \Omega_{F+})F_{\phi\theta}$ (see eq. [A18] with $\beta = -\Omega_H$), we obtain the poloidal current flowing through the horizon:

$$I_H = \frac{(r_H^2 + a^2)}{2(r_H^2 + a^2 \cos^2 \theta)} \sin \theta F_{\phi\theta} (\Omega_H - \Omega_{F+}), \quad (41)$$

Assuming the ZAMO radial magnetic field, $B_r = -F_{\phi\theta}/(\Sigma \sin \theta)$, to be independent of θ near the axis, we can calculate the total magnetic flux through the horizon in one hemisphere: $\Psi = 2\pi A_\phi = \int B_r \sqrt{g_{\phi\phi} g_{\theta\theta}} d\theta d\phi \simeq \pi \Sigma \sin^2 \theta B_r = -\pi \sin \theta F_{\phi\theta}$. Eq. (41) then yields to leading order,

$$I_H \simeq -(\Omega_H - \Omega_{F+}) A_\phi. \quad (42)$$

Likewise, the frozen-in condition at infinity gives $F_{r\theta} = \Omega_{F-} F_{\phi\theta}$, leading in the small angle approximation to,

$$I_\infty = (1/2) \sin \theta F_{\phi\theta} \Omega_{F-} \simeq -\Omega_{F-} A_\phi. \quad (43)$$

The electric charge distribution in the inner flux tube can be obtained from Maxwell's equation: $F^{t\mu}_{;\mu} = 4\pi j^t$. At small angles this equation is given, to a good approximation, by eq.

(A19) in the Appendix (cf. Van Putten 2001). Assuming as before that the ZAMO radial magnetic field is independent of θ near the axis, we obtain from eq. (A19) the Goldreich-Julian charge density:

$$\rho_e = \alpha^2 j^t = -\frac{(\Omega_F + \beta)B_r \cos \theta}{2\pi}, \quad (44)$$

where Ω_F denotes the local angular velocity of the flux-surface at hand. Evidently, the electric charge changes along the inner flux tube from $\rho_{eH} = (\Omega_H - \Omega_{F+})B_r/2\pi$ on the horizon, to $\rho_{e\infty} = -\Omega_{F-}B_r/2\pi$ at infinity, and vanish at the radius at which $-\beta = \Omega_F$, corresponding to a locally zero angular momentum state of the flux-surface. This is illustrated in fig. 4. Using eq. (A20) and (44), one finds $j^r = j^t v^r$, where $v^r = 1$ at infinity, and $v^r = -\alpha^2$ on the horizon (see Appendix). *This implies that the current on the horizon and at infinity is purely due to convection of Goldreich-Julian charges.* A similar conclusion was drawn by Punsly and Coroniti (1990).

7.2. Two steady state limits

Current closure of I_∞ through the inner tube over the outer tube with equal magnetic flux of opposite sign gives rise to a differentially rotating inner tube, described by

$$\Omega_{F+} - \Omega_{F-} = \Omega_H - 2\Omega_T \quad (45)$$

(van Putten & Levinson 2002). This assumes the force-free limit, whereby current is conserved along flux-surfaces and $I_H = I_\infty$.

Alternatively, current closure of I_∞ through the inner tube over the outer tube and the outer torus magnetosphere allows for the limit of a uniformly rotating inner tube. This corresponds to the limit of infinity conductivity. Combined with the force-free limit, this approach was used by Blandford & Znajek (1977) and Phinney (1983) to construct their force-free solutions and determine the efficiency of the energy extraction process. Near the axis Eqs. (42) and (43) yield to leading order,

$$\Omega_{F+} = \Omega_{F-} = \Omega_H/2. \quad (46)$$

It will be appreciated that this implies nearly maximal energy extraction rate on the inner tube.

Punsly & Coroniti (PC; 1990) argue that the assumption made by Blandford & Znajek (1977) and Phinney (1983), namely that the magnetosphere is force-free in the entire region between the horizon and infinity, violates the principle of MHD causality. Their argument relies on the observation that the inflow must become superfast on the horizon and, therefore,

cannot communicate with the plasma source region (e.g., the gap in the Blandford-Znajek model). They concluded that the use of the Znajek frozen-in condition on the horizon to determine Ω_F is unphysical, and that Ω_F must be determined by the dissipative process that leads to ejection of plasma on magnetic field lines. This point is of interest, as the black hole has a finite, though secular lifetime of rapid spin as an inner engine to gamma-ray bursts. In what follows we reexamine this issue.

We remark that MHD causality prohibits infinitely rigid structures (the Alfvén velocity is bounded by the velocity of light). This is true in particular over distances much larger than the system size. Nevertheless, we may examine a steady-state force-free limit $\Omega_{F+} \simeq \Omega_{F-} \simeq \Omega_H/2$ as a close approximation on scales comparable to the system size, modified only by a differentially rotating gap which injects the associated electric current in a region where frame-dragging β is pronounced.

The current flow in the inner tube is created in a slightly differentially rotating gap in a neighborhood of $\Omega_F = -\beta$ between two Alfvén surfaces. The gap size (and hence current output) is determined by the local degree of differential frame-dragging in β . As the magnetosphere around the black hole is transparent to β , the gap remains in causal contact with the angular velocity of the black hole: a change in the asymptotic value $-\beta = \Omega_H$ on the horizon is associated with a change in β throughout the surrounding spacetime. This indicates that the gap is subject to changes $\delta\Omega_H$ under general conditions.

If $I_H \neq I_\infty$, the inner tube develops a response by charge conservation: time-variable or in steady state, depending on the absence or presence of cross-field currents (i.e., j_θ) between the inner and the outer tube. Conceivably, the plasma injection process maintains the required cross-field currents, and there exist multiple current closure paths. In view of (42) and (43), note that this implies additional differential rotation in the inner tube with accompanying dissipation processes. In the absence of cross-currents, there results a time-variable adjustment of the two Alfvén surfaces which delimit the gap by application of Gauss’ theorem to, respectively, the black hole plus lower section and the upper section. This causes adjustment of the current injected into the lower and the upper sections. In steady state, this recovers $I_H = I_\infty$. This argument leaves open the possibility that the gap is time-variable, however, especially on the light crossing time-scale.

7.3. Output power through the inner tube

The inner tube releases black hole-spin energy at a certain rate, set by the horizon half-opening angle θ_H shown in Figs. 4 and 10. Forementioned force-free limits (45-46) define

bounds for the bipolar outflows of black hole-spin energy through the inner tube, i.e.,

$$\Omega_{F+}(\Omega_H - \Omega_{F+})A_{in}^2 \leq S_m \leq \frac{1}{4}\Omega_H^2 A_{in}^2, \quad (47)$$

where $2\pi A_{in}$ is the net magnetic flux on the horizon associated with the inner tube. Hence, we have a fraction

$$\frac{E_j}{E_{rot}} \simeq \frac{1}{4}\theta_H^4 \quad (48)$$

of the rotational of the black hole (see eqs. [1] and [2]).

The observed true GRB energies cluster around 3×10^{50} erg (Frail et al. 2001). This corresponds to $E_j = 2 \times 10^{51}$ erg $\times (0.16/\epsilon)$, where ϵ denotes the efficiency of conversion of kinetic energy-to-gamma rays. In our model of GRBs from rotating black holes, this observational constraint introduces the small parameter

$$\frac{E_j}{E_{rot}} \simeq 10^{-3} \left(\frac{7M_\odot}{M} \right) \left(\frac{0.16}{\epsilon} \right). \quad (49)$$

This corresponds to a horizon half-opening angle $\theta_H \geq 15^\circ$; $\theta_H \simeq 35^\circ$ associated with the output from the gap in (45).

We propose to identify θ_H with the curvature in poloidal topology of the inner torus magnetosphere (van Putten 2002b), $\theta_H \sim M/R$ within a factor close to one. In this event, we have

$$\frac{E_j}{E_{rot}} \sim \frac{1}{4} \left(\frac{M}{R} \right)^4. \quad (50)$$

A spread in torus radius by a factor of about two corresponds to a spread in energies in baryon-poor outflows by about one order of magnitude, consistent with the observed spread in true GRB energies.

The fate of the Poynting flux-outflow is determined by specific mechanisms for dissipation, as these may arise downstream of the upper section of the open flux-tube.

8. Structure of the outer tube

The open field lines that are anchored to the torus form the outer flux tube. The baryon-rich material ejected from the torus, derived from the spin-energy of the black hole (see §6), flows along those open field lines to infinity. We have estimated this to constitute

a substantial mass loss. In the ideal MHD approximation the angular velocity of the outer flux-tube is conserved along magnetic field lines (on the scale of the system) and, therefore, equals that of the torus, viz., $\Omega_F = \Omega_T$. Above the Alfvén point the ratio of toroidal and poloidal field in the outflow is (see eq [A11] with $\Omega_F = \Omega_T$ and $v_\phi \rightarrow r^{-1}$)

$$\frac{F_{r\theta}}{F_{\phi\theta}} = \frac{\Omega_T}{v_r}. \quad (51)$$

As argued above, the direction of the poloidal magnetic field in the outer flux tube is opposite to its direction in the inner tube. Thus, if the torus and the black hole rotate in the same direction, as envisioned here, then the toroidal magnetic field $F_{r\theta}$ have opposite orientations in the inner and outer tubes. The Goldreich-Julian charge density in the outer tube is

$$\rho_e = \frac{\Omega_T B_r \cos \theta}{2\pi}, \quad (52)$$

and is opposite in sign to the outflowing charges in the inner flux tube. These charges carry the current flowing along the open field lines from the torus. This region of the torus magnetosphere is equivalent to a pulsar magnetosphere.

We conclude that the outer tube forms out of the outer layers of the inner torus magnetosphere (the magnetic wall around the black hole), and joins the open field-lines in the outer torus magnetosphere in creating a super-Alfvénic baryon-rich wind to infinity. It conceivably contributes to collimation of the baryon-poor outflows in the inner flux-tube.

9. The interface between the inner and the outer flux-tube

The creation of the open magnetic flux tubes from the closed torus magnetosphere topologically represents folding of magnetic field lines in the upper section of the inner/outer flux-tube, which gives rise to an antiparallel orientation of the poloidal magnetic field. This is accompanied by a cylindrical current and charge sheet that accounts for the jump in the electric and magnetic fields across the interface. The lower section of the inner/outer flux-tube which connects to the horizon has, instead, a parallel orientation between the poloidal magnetic field. In the perfect MHD limit, the properties of the interface are described by jump conditions as follow from Maxwell's equations, $F^{t\mu}_{;\mu} = 4\pi j^t$, i.e.:

$$4\pi\sigma_e = [\Omega r \sin \theta B_r] = r \sin \theta \Omega_T B_{r+} - r \sin \theta (\Omega_H/2) B_{r-}, \quad (53)$$

where B_{r+} (B_{r-}) denotes the radial magnetic field near the interface in the outer (inner) flux tube. The poloidal and toroidal interface currents are, likewise,

$$\begin{aligned} 4\pi J^r &= [B_\phi] = \left[\frac{\Omega r \sin \theta B_r}{v^r} \right], \\ 4\pi J^\phi &= -[B_r]. \end{aligned} \quad (54)$$

The poloidal current (54) results beyond the Alfvén point, where the wind transports angular momentum outwards to infinity. The outflow in the inner tube is expected to be relativistic ($v^r = 1$). If the baryon rich outflow from the torus also becomes relativistic, then the latter equation imply that $J^r = \sigma_e$, namely the poloidal current in the boundary layer is solely due to the outflowing surface charges. The poloidal current sheet – possibly further carrying a poloidal current – is a potential site for reconnection of magnetic field lines, which would convert magnetic energy in the inner flux tube into kinetic energy.

9.1. Dissipation in the folded upper section of the flux-tubes

The upper interface between the inner and the outer flux tubes is subject to antiparallel magnetic fields and strong differential rotation (whenever $\Omega_T \neq \Omega_H/2$). It is therefore a potential site for reconnection of magnetic field lines, and may give rise to conversion of a fraction of the magnetic energy in the inner flux tube into kinetic energy. In order to assess the fraction of magnetic energy which is converted in the interface, a detailed reconnection model is required. Here, we point out that the reconnection time is limited by the crossing time of an Alfvén wave across the inner tube, which is typically very short. If this limit applies then an appreciable fraction of magnetic energy will be dissipated. (The reconnection rate could be much smaller.) In any case, the power extracted from the hole by the inner tube is uncertain, because the angular velocity of the inner tube on the horizon is unknown. In or near the lowest energy state of the gap, the inner tube mediates a power S_m , as given by eq. (47).

The electric fields produced by the reconnection process in the interface may inject plasma, including baryons that should be present in the boundary layer, into the inner tube. This would lead to mass loading of the inner tube and additional conversion of the Poynting flux. The amount of baryonic contamination by this process is yet an open issue.

Additional dissipation may arise from a differential rotation of the inner flux tube, as discussed in (van Putten & Levinson 2002). It is clear that if the system fluctuates over a time scale Δt , then nonlinear disturbances may induce differential rotation over length scales $< c\Delta t$ (which corresponds to 10^4 gravitational radii for the entire life time of the system). Such electromagnetic fronts should be highly dissipative by virtue of the large parallel electric fields associated with the differential rotation of the magnetic flux tubes. It is anticipated that, under the conditions envisioned here, copious pair and photon productions would ensue inside the differentially rotating fronts.

10. Observational consequences

We have described in some detail the topology, lifetime and emissions of black hole-torus systems in the suspended accretion state. Fig. 11 summarizes the energy transport and conversion of black hole-spin energy, catalyzed by the torus. Most energy is dissipated in the horizon, while the major output is converted by the torus into gravitational radiation, winds and neutrino emissions (as well as thermal emissions). A minor output is released in baryon-poor outflows as input to the observed GRB-afterglows. The analysis is based largely on equivalence to pulsar magnetospheres. The suspended accretion state develops against a magnetic wall around rapidly rotating black holes. This is based on a uniform magnetization of the torus, represented by two oppositely oriented current rings in a torus formed in black hole-neutron star coalescence and core-collapse hypernovae.

The proposed emissions in gravitational radiation are powered by the spin-energy of the black hole, which renders these emissions a powerful new source for the upcoming gravitational wave-experiments. This output is contemporaneous with GRBs from baryon poor outflows, and hence have the same durations as the redshift corrected durations of long GRBs – tens of seconds, due to the condition of magnetic stability of the torus.

Calorimetry on the emissions in gravitational radiation provides a rigorous compactness test for Kerr black holes (van Putten 2001a), which can be pursued by upcoming gravitational wave-experiments. We emphasize that our predictions on the energies and duration of emissions in gravitational radiation are robust and are independent of an association with GRBs. Hypernovae could be over-abundant as burst sources of gravitational radiation, with only a small fraction making successful GRBs. Calorimetry on wind energies provides a method for constraining the angular velocity of the torus and, hence, its quadrupole emissions in gravitational radiation. Possible channels are recently observed X-ray line emissions in GRB 011211 (Reeves et al. 2002), hypernova remnants – which remain to be identified – and by association with soft X-ray transients with chemically enhanced companion stars (Brown et al. 2000).

X-ray and radio shells that may result from the interaction of the baryon rich torus winds with ambient matter, as well as the gamma-ray emission expected to be produced by the baryon poor outflows in the inner tube, should be sought for (Levinson et al. 2002).

Below we summarize our findings and draw additional conclusions:

1. Most of the black hole-luminosity is incident on the torus by topological equivalence to pulsar magnetospheres, when the black hole spins rapidly. We identify a new magnetic instability, which defines a minimum lifetime T of tens of seconds of the spin of the black

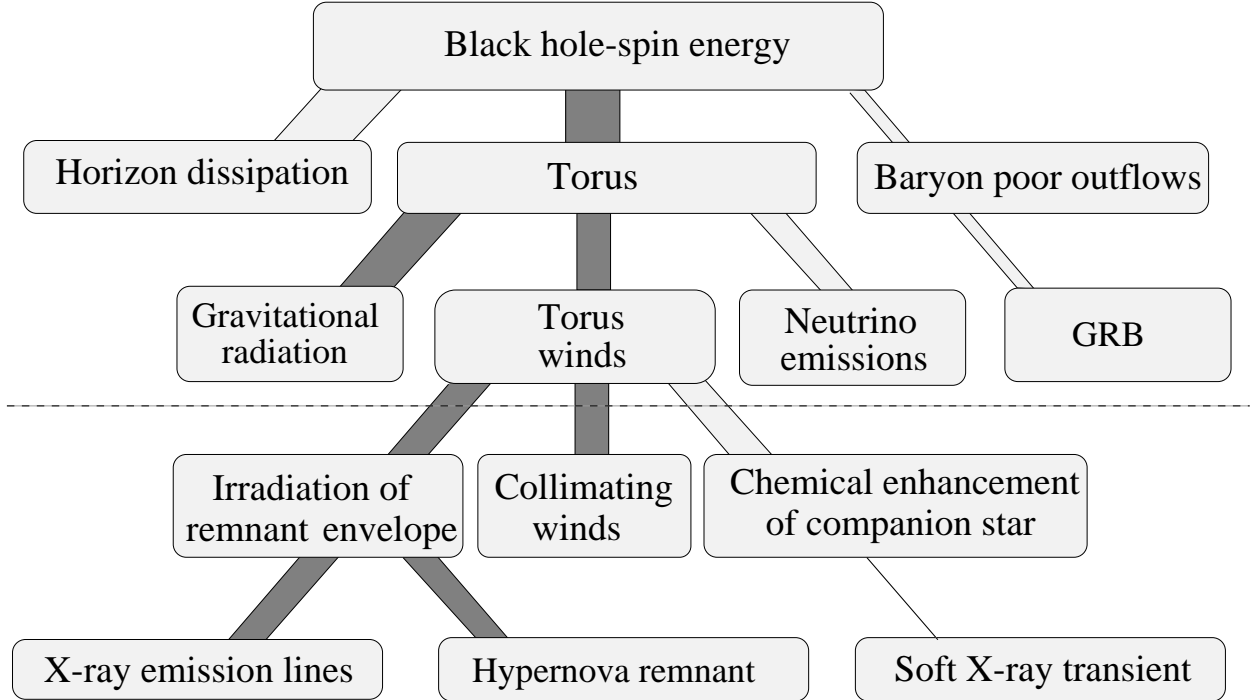


Fig. 11.— Overview of energy transport and conversion of black hole-spin energy catalyzed by a uniformly magnetized torus. Most of the spin-energy is dissipated in the horizon – an unobservable sink of energy – at a rate which is limited by a new magnetic stability criterion for the torus. This process effectively defines the lifetime of rapid spin of the black hole. Most of the spin-energy released is incident on the inner face of the torus, while a minor fraction forms baryon-poor outflows through the inner flux-tube to infinity. We associate the latter with the input to the observed GRB-afterglow emissions. The torus converts its input primarily into gravitational radiation and, to a lesser degree, into winds, thermal and neutrino emissions. Direct measurement of the energy and frequency emitted in gravitational radiation by the upcoming gravitational wave-experiments provides a calorimetric compactness test for Kerr black holes (dark connections). Channels for calorimetry on the torus winds are indicated below the dashed line, which are incomplete or unknown. They provide in principle a method for constraining the angular velocity of the torus and its frequency of gravitational radiation. This is exemplified by tracing back between torus winds and their remnants (dark connections). As the remnant envelope expands, it reaches optical depth of unity and releases the accumulated radiation from within. This continuum emission may account for the excitation of X-ray line emissions seen in GRB 011211, which indicates a torus wind energy of a few times 10^{52} erg. Matter ejecta ultimately leave remnants in the host molecular cloud, which remain to be identified. Torus winds may further deposit a fraction of their mass onto the companion star (Brown et al. 2000), thereby providing a chemical enrichment in a remnant soft X-ray transient.

hole, corresponding to a large system parameter $T/M \sim 10^6$.

2. At MeV temperatures of the torus, a torus with a minor radius of less than about the linear size of the black hole becomes unstable to the formation of a finite multipole mass moments by the Papaloizou-Pringle instability and, conceivably, other modes. The torus hereby converts a major fraction $E_{gw}/E_{rot} \simeq 10\%$ into gravitational radiation, conceivably at multiple lines. At a source distance of 100Mpc, these emissions over $N = 2 \times 10^4$ periods give rise to a characteristic strain amplitude $\sqrt{N}h_{char} \simeq 6 \times 10^{-21}$ (Coward et al. 2002).

3. A minor fraction $E_j/E_{rot} \sim 10^{-3}$ of black hole-spin energy is released in baryon poor outflows. We attribute this fraction to curvature in poloidal topology, whereby $E_j/E_{rot} \simeq (1/4)(M/R)^4$ is standard for a universal horizon half-opening angle $\theta_H \simeq M/R$ of the associated open magnetic flux-tube. These outflows are probably not high-sigma – the ratio of Poynting flux-to-kinetic energy flux – owing, in part, to magnetic reconnection in an interface with baryon-rich winds flowing along the surrounding outer flux-tube.

4. Causality in the process of spin-up of the torus by the black hole follows by topological equivalence to pulsar magnetospheres (van Putten 1999). In response, the black hole spins down by conservation of energy and angular momentum. This establishes causality in the extraction of black hole-spin energy by horizon Maxwell stresses as proposed by Blandford & Znajek (1977). Causality in the formation of baryon poor outflows from the open magnetic flux-tube is due to transparency of the magnetosphere to the gravitational field: the associated current injection is subject to current continuity between asymptotic boundary conditions on the horizon and at infinity by Gauss’ theorem, and regulated by differential frame-dragging and current closure at infinity.

5. Calorimetry on the predicted energy output in gravitational radiation by the upcoming gravitational wave experiments provides a method for identifying Kerr black holes as objects in nature when $2\pi \int_0^{E_{gw}} f_{gw} dE > 0.005$ (van Putten 2001a), where f_{gw} denotes the quadrupole frequency of gravitational waves. Current experiments consist of laser interferometric detectors LIGO, VIRGO, TAMA and GEO, bar and sphere detectors. An individual source is band limited in gravitational radiation in terms of a frequency sweep of about 10%, corresponding to emission of the first 50% of the output in gravitational radiation from a maximally spinning Kerr black hole. Collectively, black hole-torus systems are conceivably luminous in multiple frequencies with broad distributions owing to a spread in black hole mass.

6. Frequencies of quadrupole gravitational radiation $f_{gw} \simeq 470\text{Hz} (E_w/4 \times 10^{52}\text{erg})^{1/2} (7M_\odot/M_H)^{3/2}$ can be predicted by calorimetry on the torus wind energies E_w . Calorimetry on X-ray line emissions point towards frequencies around 500Hz (van Putten 2002b).

7. Calorimetry on E_w may also be pursued by calorimetry on hypernova remnants, given the observed supernova association (e.g., Bloom et al. (2002)). Our model suggests the ejection of the remnant stellar envelope as a shell with kinetic energy $0.5\beta E_w \sim 3 \times 10^{51} \text{erg}(\beta/0.1)(M_H/10M_\odot)(\eta/0.1)$. Here, β denotes the initial radial velocity β relative to the velocity of light, in response to the impact of E_w from within. For a supernova association to molecular clouds, see, e.g., Chu & MacLow (1990); Wang & Helfand (1991); a hypernova or gamma-ray burst association to molecular clouds has been considered by Efremov et al. (1998); Wang (1999); Dunne et al. (2001); Lai et al. (2001); Chen et al. (2002); Price et al. (2002). Determining kinetic energies of these remnants can be pursued analogously to studying supernova remnants, in the radio and X-ray. Chandra-X observations may hereby identify hypernova remnants in X-ray bright (super)shells around a black hole-binary, possibly in the form of a soft X-ray transient.

Acknowledgement. The first author acknowledges constructive comments from G. Mendell and B.-C. Koo. This research is supported by NASA Grant 5-7012, a NATO Collaborative Linkage Grant and an MIT C.E. Reed Fund. The LIGO Observatories were constructed by the California Institute of Technology and Massachusetts Institute of Technology with funding from the National Science Foundation under cooperative agreement PHY 9210038. The LIGO Laboratory operates under cooperative agreement PHY-0107417. This paper has been assigned LIGO Document Number LIGO-P020030-00-R.

REFERENCES

- Abramovici, A., et al., Science, 256, 325
- Balbus, Hawley, J., 1992, ApJ, 400, 610
- Bethe, H.A., & Wilson, J.R. 1985, ApJ, 295, 14
- Blandford, R.D., & Znajek, W.L., 1977, MNRAS, 179, 377
- Blandford, R.D., & Payne, D.G. 1982, MNRAS, 199, 883
- Bloom, J.S., et al., 2002, ApJ, Lett., submitted
- Bradaschia, C., et al., Phys. Lett. A., 163, 15
- Brown G.E., Lee, C.-H., Wijers, R.A.M.J., Lee, H.K., Israelian, G., & Bethe, H.A., 2000, NewA, 5, 191
- Camenzind, M. 1986, A&A, 162, 32

- Chen, C.-H. Rosie, et al., 2002, AJ, 123, 2462
- Chu, Y.-H., & MacLow, M.-M., 1990, ApJ, 365, 510
- Coward, D., van Putten, M.H.P.M., & Burman, R., 2002, ApJ, 580, 1024
- Cohen, J.M., Kegeles, L.S., Rosenblum, A., 1974, ApJ, 201, 783
- Dunne, B.C., Points, S.D., & Chu, Y.-H., 2001, ApJ, 136, 119
- Efremov, Y.N., Elmegreen, B.G., Hodge, P.W., 1998, ApJ, 501, L163
- Eichler, D., Livio, M., Piran, T., & Schramm, D.N. 1989, Nature, 340, 126 APS April/HEAD
AAS Meeting, Albuquerque, NM
- Frail et al., 2001, ApJ, 562, L55
- Goldreich, P.M., & Julian, W.H., 1969, ApJ, 157, 869
- Hirotsu, K., Takahashi, M., Nitta, S., & Tomimatsu, A. 1992, ApJ, 386, 455
- Jackson, J.D., 1975, *Classical electrodynamics* (Wiley & Sons, Inc.), §5.5
- Lai, S.-P., et al., 2001, ApJ, 547, 754
- Levinson, A. & Eichler D., 1993, ApJ, 418, 386
- Levinson, A., et al., 2002, ApJ, 576, 923
- Masaki, A., et al., 2001, Phys. Rev. Lett., 86, 3950
- Miller, J.M., Fabian, A.C., Wijnands, R., Reynolds, C.S., Ehle, M., Freyberg, M.J., van der
Klis, M., Lewin, W.H.G., Sanchez-Fernandez, C., Castro-Tirado, A.J., 2002, ApJ,
570, L69
- Kerr, R.P., 1963, Phys. Rev. Lett., 11, 237
- Paczynski, B.P., 1991, Acta Astron., 41, 257
- Paczynski, B.P., 1998, ApJ, 494, L45
- Papaloizou, J.C.B., & Pringle, J.E., 1984, MNRAS, 1984, 208, 721
- Phinney, E.S., 1983, in *Astrophysical Jets*, ed. A. Ferrari & A.G. Pacholczyk (Dordrecht:
Reidel), 201

- Price, P.A., et al., 2002, astro-ph/0208008; submitted
- Punsly, B., & Coroniti, F.V. 1990, ApJ, 350, 518
- Reeves, J.N., et al., 2002, Nature, 416, 512
- Romanova, M.M., Ustyugova, G.V., Koldoba, A.V., Chechetkin, V.M., & Lovelace, R.V.E., 1997, ApJ, 482, 708
- Schutz, B.F., & Papa, M.A., 1999, gr-qc/9905018
- Takahashi, M., Nita, S., Tatematsu, Y., & Tominatsu, A. 1990, ApJ, 363, 206
- Thorne, K.S., Price, R.H., & Macdonald, D.A. 1986, Black Holes: The Membrane Paradigm. Yale University Press.
- M.H.P.M. van Putten, 1999, Science, 284, 115
- van Putten M.H.P.M. & Ostriker, E.C., 2001, ApJ, 552, L31
- van Putten, M.H.P.M., 2001b, ApJ, 562, L51
- van Putten, M.H.P.M., 2001a, Phys. Rep., 345, 1
- van Putten M.H.P.M. & Levinson, A., 2002, Science, 295, 1874; published online 21 February 2002; 10.1126/science.1068634
- van Putten, M.H.P.M., 2002, ApJ, 575, L71
- van Putten, M.H.P.M., 2002, ApJ, 583, to appear
- Wilms, J., Reynolds, C., Begelman, M.C., Reeves, J., Silvano, M., Rüdiger, S., & Eckard, K., 2001, MNRAS, 328, L27
- Wang, Q.D., & Helfand, D.J., 1991, ApJ, 373, 497
- Wang, Q.D., ApJ, 517, L27
- Woosley, S.E., 1993, ApJ, 405, 273
- Znajek, W.L., 1977, MNRAS, 179, 457

A. Ideal MHD in Kerr geometry

We express the Kerr metric in Boyer-Lindquist coordinates with the following notation:

$$ds^2 = -\alpha^2 dt^2 + \tilde{\omega}^2 (d\phi + \beta dt)^2 + \frac{\rho^2}{\Delta} dr^2 + \rho^2 d\theta^2, \quad (\text{A1})$$

where $\alpha = \rho\sqrt{\Delta}/\Sigma$ is the lapse function, $\tilde{\omega}^2 = (\Sigma^2/\rho^2)\sin^2\theta$, $-\beta = 2aMr/\Sigma^2$ is the angular velocity of a ZAMO with respect to a distant observer, with $\Delta = r^2 + a^2 - 2Mr$, $\rho^2 = r^2 + a^2\cos^2\theta$, and $\Sigma^2 = (r^2 + a^2)^2 - a^2\Delta\sin^2\theta$. The parameters M and a are the mass and angular momentum per unit mass of the black hole.

We denote by n , p , ρ , $h = (\rho+p)/n$, the proper particle density, pressure, energy density, and specific enthalpy, respectively. The stress-energy tensor then takes the form:

$$T^{\alpha\beta} = hnu^\alpha u^\beta - pg^{\alpha\beta} + \frac{1}{4\pi}(F^{\alpha\sigma}F_\sigma^\beta + \frac{1}{4}g^{\alpha\beta}F^2), \quad (\text{A2})$$

where u^α is the four-velocity, and $F_{\mu\nu}$ is the electromagnetic tensor which satisfies Maxwell equations. The dynamics of the MHD flow is then governed by the equation

$$T^{\mu\nu}_{;\nu} = 0, \quad (\text{A3})$$

subject to conservation of particle flux,

$$(nu^\alpha)_{;\alpha} = \frac{1}{\sqrt{-g}}(\sqrt{-g}nu^\alpha)_{;\alpha} = 0. \quad (\text{A4})$$

The ideal MHD assumption (i.e., infinite conductivity) imposes the additional constraint,

$$u^\alpha F_{\alpha\beta} = 0. \quad (\text{A5})$$

The stationary axisymmetric flow considered here is characterized by two Killing vectors: $\xi^\mu = \partial_t$ and $\chi^\mu = \partial_\phi$. By contracting with the stress-energy tensor we can construct the energy and angular momentum currents: $\mathcal{E}^\alpha = T^\alpha_\beta \xi^\beta = T^\alpha_t$, and $\mathcal{L}^\alpha = T^\alpha_\beta \chi^\beta = T^\alpha_\phi$, which are conserved, viz.,

$$\mathcal{L}^\alpha_{;\alpha} = \mathcal{E}^\alpha_{;\alpha} = 0. \quad (\text{A6})$$

Equations (A4), (A5), and (A6) together with the homogeneous Maxwell equations admit 4 quantities that are conserved along magnetic flux surfaces, the shape of which is given by a stream function $\Psi(r, \theta)$: The particle flux per unit magnetic flux,

$$\eta(\Psi) = \frac{\sqrt{-g}nu^r}{F_{\theta\phi}} = \frac{\sqrt{-g}nu^\theta}{F_{\phi r}}. \quad (\text{A7})$$

The angular velocity of magnetic field lines,

$$\Omega_F(\Psi) = F_{tr}/F_{r\phi} = F_{t\theta}/F_{\theta\phi}. \quad (\text{A8})$$

The total energy and angular momentum per particle carried by the MHD flow,

$$E(\Psi) = hu_t - \frac{\sqrt{-g}}{4\pi\eta}\Omega_F F^{r\theta}, \quad (\text{A9})$$

$$L(\Psi) = -hu_\phi - \frac{\sqrt{-g}}{4\pi\eta}F^{r\theta}. \quad (\text{A10})$$

The above equations also yield the relation

$$\frac{F_{r\theta}}{F_{\phi\theta}} = \frac{\Omega_F - v^\phi}{v^r}, \quad (\text{A11})$$

where $v^\phi = u^\phi/u^t$, and $v^r = u^r/u^t$ are the corresponding components of the 3-velocity. Equations (A9) and (A10) can be used to express u^t , v^ϕ , and $F^{r\theta}$ in terms of E , L , and the Alfvén Mach number, defined by $M^2 = 4\pi h\eta^2/n$. One finds

$$F_\theta^r = \frac{4\pi\eta}{\sin\theta} \frac{(g_{tt} + g_{t\phi}\Omega_F)L + (g_{t\phi} + g_{\phi\phi}\Omega_F)E}{k_0 + M^2}, \quad (\text{A12})$$

$$hu^t = h(-u_t + \beta u_\phi)/\alpha^2 = (E - \Omega_F L) - \frac{M^2(E + \beta L)}{\alpha^2(k_0 + M^2)}, \quad (\text{A13})$$

$$v^\phi = \frac{-\alpha^2 g_{\phi\phi}\Omega_F(E - \Omega_F L) + M^2(g_{t\phi}E + g_{tt}L)}{-\alpha^2 g_{\phi\phi}(E - \Omega_F L) - M^2(g_{\phi\phi}E + g_{t\phi}L)}, \quad (\text{A14})$$

where $k_0 = g_{tt} + 2g_{t\phi}\Omega_F + g_{\phi\phi}\Omega_F^2$. Finally, using the normalization condition, $u^\mu u_\mu = -1$, we obtain for the poloidal velocity, defined as $u_p^2 = u_r u^r + u_\theta u^\theta$, the relation

$$u_p^2 + 1 = (\alpha u^t)^2 - (u_\phi/\tilde{\omega})^2. \quad (\text{A15})$$

Note that u_p is the poloidal 4-velocity as measured by a ZAMO, and αu^t is the corresponding t component of the 4-velocity. As seen, the Lorentz factor of the inflow in the ZAMO frame approaches $\Gamma = \alpha u^t \sim \alpha^{-1}$ on the event horizon.

Consider first the behavior of the solution near the horizon. There $\alpha \rightarrow 0$ and so

$$v^\phi \rightarrow -\frac{(g_{t\phi}E + g_{tt}L)}{(g_{\phi\phi}E + g_{t\phi}L)} = \Omega_H. \quad (\text{A16})$$

The poloidal velocity is radial on the horizon, implying $u_p^2 \rightarrow g_{rr}u^r u^r$. Using eq. (A15) we find,

$$v^r = u^r/u^t \rightarrow \alpha/\sqrt{g_{rr}} = -\Delta/(r^2 + a^2). \quad (\text{A17})$$

Substituting the above results into eq. (A11), we finally obtain,

$$\frac{F_{r\theta}}{F_{\phi\theta}} = -\frac{r^2 + a^2}{\Delta}(\Omega + \beta). \quad (\text{A18})$$

Eq. (A18) gives the boundary condition on the horizon.

The Boyer-Lindquist electric charge density in the flow is determined from Maxwell's equation: $F^{t\mu}_{;\mu} = 4\pi j^t$. It can be readily shown that if the poloidal component of the magnetic field is radial on the event horizon (which is the case in the force-free limit of an uncharged black hole), then near the horizon the later equation reduces to,

$$\frac{\partial}{\partial\theta} \left[\frac{\sin\theta}{\alpha^2}(\Omega + \beta)F_{\phi\theta} \right] = 4\pi\sqrt{-g}j^t. \quad (\text{A19})$$

The poloidal current follows from the equation,

$$\frac{\partial}{\partial\theta} \left(\frac{\sin\theta}{\rho^2}F_{r\theta} \right) = 4\pi\sqrt{-g}j^r. \quad (\text{A20})$$

Using eqs. (A11), (A16), (A19), and (A20), we finally recover the result (Punsly & Coroniti 1990))

$$j^r = \frac{\rho_e}{v_p}, \quad (\text{A21})$$

where $\rho_e = \alpha^2 j^t$, and $v_p = u_p/u_{\hat{t}}$ being the three velocity as measured by a ZAMO.